NASA TECHNICAL MEMORANDUM


NASA TM X-2239

NASA TM X-2239

# EXPERIMENTAL INVESTIGATION OF THE EFFECT OF SCREEN-INDUCED TOTAL-PRESSURE DISTORTION ON TURBOJET STALL MARGIN

*by James E. Calogeras, Charles M. Mehalic, and Paul L. Burstadt*

*Lewis Research Center*
*Cleveland, Ohio 44135*

NATIONAL AERONAUTICS AND SPACE ADMINISTRATION • WASHINGTON, D. C. • MARCH 1971

| 1. Report No. NASA TM X-2239 | 2. Government Accession No. | 3. Recipient's Catalog No. |
|---|---|---|
| 4. Title and Subtitle EXPERIMENTAL INVESTIGATION OF THE EFFECT OF SCREEN-INDUCED TOTAL-PRESSURE DISTORTION ON TURBOJET STALL MARGIN | | 5. Report Date March 1971<br>6. Performing Organization Code |
| 7. Author(s) James E. Calogeras, Charles M. Mehalic, and Paul L. Burstadt | | 8. Performing Organization Report No. E-5981<br>10. Work Unit No. 720-03 |
| 9. Performing Organization Name and Address Lewis Research Center<br>National Aeronautics and Space Administration<br>Cleveland, Ohio 44135 | | 11. Contract or Grant No.<br>13. Type of Report and Period Covered Technical Memorandum |
| 12. Sponsoring Agency Name and Address National Aeronautics and Space Administration<br>Washington, D.C. 20546 | | 14. Sponsoring Agency Code |

15. Supplementary Notes

16. Abstract

The effect of several circumferential, radial, and combined distortions on the stall margin of a J85-GE-13 turbojet engine was investigated. The compressor was found to have a critical angle of circumferential distortion equal to $60^{\circ}$. For both single and multiple circumferential distortions, loss in compressor pressure ratio at stall was correlated with a simple distortion index based on the lowest mean pressure in any $60^{\circ}$ sector of the compressor face flow field. Hub radial distortion was found to affect the pumping capacity and pressure ratio of the compressor, but not stall margin; however, tip radial distortion did affect the stall margin. The circumferential component of a combined pattern was generally found to be the predominant factor affecting stall margin.

| 17. Key Words (Suggested by Author(s)) | 18. Distribution Statement |
|---|---|
| Distortion index<br>Total pressure distortion<br>Stall margin<br>Compressor sensitivity to distortion<br>Effect of distortion on compressor | Unclassified - unlimited |

| 19. Security Classif. (of this report) | 20. Security Classif. (of this page) | 21. No. of Pages | 22. Price* |
|---|---|---|---|
| Unclassified | Unclassified | 55 | $3.00 |

*For sale by the Clearinghouse for Federal Scientific and Technical Information
Springfield, Virginia 22151

# EXPERIMENTAL INVESTIGATION OF THE EFFECT OF SCREEN-INDUCED TOTAL-PRESSURE DISTORTION ON TURBOJET STALL MARGIN

by James E. Calogeras, Charles M. Mehalic, and Paul L. Burstadt

Lewis Research Center

## SUMMARY

An experimental investigation was made to determine the effects of screen-induced total-pressure distortions on a J85-GE-13 turbojet engine. Radial and circumferential screen patterns of various extents and intensities were tested, both separately and in combination. Results indicate the compressor to be sensitive to a critical angle of circumferential distortion equal to $60^{\circ}$. For both single and multiple circumferential distortions, loss in compressor pressure ratio at stall was correlated with a distortion index based on the lowest mean pressure in any $60^{\circ}$ sector of the compressor face flow field. Hub radial distortion was found to affect the pumping capacity and pressure ratio of the compressor, but not the stall margin; however, tip radial distortion did affect the stall margin. The circumferential component of a combined pattern was generally found to be the predominant factor affecting stall margin.

## INTRODUCTION

In recent years a great deal of attention has been focused on problems associated with inlet-engine compatibility. Particular attention has been paid to compressor-face total pressure fluctuations produced in supersonic inlets. These fluctuations result in total pressure distortions that may cause serious stall margin degradation if the distortion pattern persists for a time interval equal to a fraction of a rotor revolution. In any given instance of in-flight compressor stall, the stall inducing distortion will probably be neither purely radial nor purely circumferential. Rather, it will be some combination of radial and circumferential distortions, be of a certain size, shape, and intensity, and will have existed for a certain time interval. To better evaluate the inlet portion of a proposed propulsion system, then, it has become necessary to know the effect of all of these distortion variables on the performance of the engine in question.

One method now commonly used to analyze the effects of circumferential pressure distortion on compressor performance is the "parallel compressor theory" suggested by Pearson and McKenzie in reference 1. This theory divides a compressor subjected to pressure distorted inflow into parallel compressors, each with an undistorted inflow of different total pressure. It is assumed that each compressor operates on the same undistorted compressor characteristic, that there are no crossflows between compressors, and that the compressors discharge to a constant and uniform static pressure. In reference 2 the authors found this theory to be quite useful in determining the effects of circumferential pressure distortion on compressor performance when the rotors were not stalled. In the work presented in reference 3 this theory was extended to include both different types of compressors and more complex distortion patterns. In addition, a simple distortion index was developed in reference 3 from findings which showed the compressor to be sensitive to a critical angle of circumferential distortion. This critical angle is related to the minimum time required for a compressor to respond to a distortion in a steady-state manner.

Several inlet-engine compatibility studies have been made at the NASA Lewis Research Center (e.g., refs. 4 to 7). One of these studies, results of which are as yet unpublished, was conducted in the 10- by 10-Foot Supersonic Wind Tunnel to measure instantaneous distortion and its effect on the stall margin of a J85-GE-13 turbojet engine. To quantitatively interpret these results, however, it was first necessary to determine the sensitivity of this particular engine to steady-state distortion.

This report presents the results of an experimental investigation made to determine the effect of steady-state total-pressure distortion on the J85-GE-13 turbojet engine. Steady-state distortions were produced by placing screens approximately one engine diameter upstream of the compressor face. The program included varying the extent and intensity of both circumferential and radial distortions. Some combined distortion patterns were also studied in order to develop a distortion index which would apply to this engine regardless of the complexity of a pressure distortion presented it. Like reference 3, the evolution of this index for circumferential distortions was based on the determination of the critical angle of spoiling for the J85-GE-13 engine. This investigation was conducted in the Propulsion Systems Laboratory Altitude Chamber of the NASA Lewis Research Center.

## APPARATUS AND PROCEDURE

### Installation

The installation of the J85-GE-13 turbojet engine in the Propulsion Systems Labora-

tory Altitude Chamber is shown in figure 1. A photograph of the engine installation is presented in figure 1(a). Figure 1(b) is a schematic drawing detailing the more pertinent measuring stations. A direct-connect installation was utilized, with the engine mounted on a thrust stand within the chamber and the engine inlet duct passing through a labyrinth seal in the forward bulkhead. The inlet air bellmouth was designed to have a throat Mach number of 0.6 at rated engine airflow. The flow coefficient had previously been found to be repeatable to within ±0.3 percent (see ref. 8).

The General Electric J85-GE-13 is an afterburning turbojet engine possessing a high thrust-to-weight ratio. The engine consists of an eight-stage axial-flow compressor coupled directly to a two-stage turbine. It incorporates controlled compressor interstage bleed and variable inlet guide vanes, a through-flow annular combustor, and an afterburner (not used in this test) with a variable area primary exhaust nozzle. The engine inlet diameter is 16.1 inches (40.9 cm).

The variable inlet guide vanes are mechanically linked to the compressor interstage bleed valves so that when the inlet guide vanes are fully closed, the bleed valves are fully open. Normally, compressor interstage bleed was scheduled linearly from full open at 80 percent corrected engine rotor speed to full closed at 94 percent corrected speed. For all testing during this investigation, interstage bleed was rescheduled to provide linear variation between 76 and 90 percent corrected engine speeds. This schedule corresponds to the maximum allowable bleed closure for safe engine operation and was required to obtain many of the stalls at corrected speeds below 94 percent of rated speed.

The compressor was stalled by slowly closing the exhaust nozzle. In order to avoid overtemperaturing the turbine during this procedure, the first-stage turbine nozzle was approximately 26 percent smaller in area than the standard unit. At any point on the compressor map, then, the turbine was matched to the compressor at a lower turbine inlet temperature.

For this investigation the exhaust nozzle area was manually controlled. During certain portions of the test program, however, the required exhaust nozzle area was less than the minimum obtainable with the standard nozzle. To obtain the required areas, six airflow blockage plates were installed inside the nozzle leaves.

A tabulation of the screen patterns used in this investigation is presented in table I. (Symbols are defined in appendix A.) The mesh number associated with the screens indicates the number of wires in each linear inch of the square grid. The ratio $P_{min,2}/\bar{P}_1$ is indicative of the total-pressure drop across both the distortion screen and its support structure. A number 1 mesh grid structure was used to support the distortion screens. This grid structure had wire diameters of 0.080 inch (0.203 cm) and a porosity of 84.6 percent open area. It was located 16.85 inches (42.80 cm), about one compressor face diameter, upstream of the inlet guide vanes. At military rated speed the support grid produced a total-pressure difference $(P_{max} - P_{min})_2$ of about 4 percent of the compres-

sor face average total pressure. Finally, the engine bullet-nose was extended to an axial position just upstream of the screen location. Photographs of the bullet-nose extension and screen pattern number 25 are presented as figures 1(c) and (d).

## Instrumentation

Details of the steady-state pressure and temperature instrumentation used in the data analysis are presented in figure 2. The compressor face instrumentation was located 3.50 inches (8.89 cm) upstream of the inlet guide vanes. This left an axial distance of 13.35 inches (33.91 cm), or slightly less than one compressor face diameter, between the distortion screens and the compressor face instrumentation. The five total pressure probes of each compressor face rake were area weighted radially and each probe represented a $60^{\circ}$ circumferential sector. During analysis, an adjustment in the data corresponding to one or more probes on a compressor face rake was found to be necessary whenever a distortion screen boundary coincided with these probes. This was required because the low pressure region tended to diffuse slightly during the transport time from screen to probe, just covering a probe that might be coincident with the actual screen boundary. To properly weight such a probe, a pressure was assigned it equal to the average of the two immediately adjacent probes at the same radius. An adjustment was also made to the probes centrally immersed in the spoiled flow sector of screen pattern number 10, a $30^{\circ}$ circumferential distortion pattern. These probes were assigned a $30^{\circ}$ circumferential sector representation. Each of the immediately adjacent probes at the same radius was assigned an additional $15^{\circ}$ circumferential sector representation. The positions of the screens relative to the compressor face total-pressure rakes are indicated in subsequent figures.

## Test Procedure

Atmospheric air was supplied to the inlet duct and was throttled to a total pressure of 10 pounds per square inch (68 948 $N/m^2$) in order to obtain a nominal Reynolds number index ReI of 0.70 at the compressor face. This value corresponded to the ReI associated with the inlet-engine compatibility tests referred to in the INTRODUCTION. Because of atmospheric temperature variations and distortion screen pressure losses, the actual compressor face ReI fluctuated approximately 10 percent about an average value 0.67. The altitude chamber pressure $P_0$ was maintained at 4.5 pounds per square inch (31 026.6 $N/m^2$). This was just low enough to ensure exhaust nozzle operation at critical flow for all engine operating conditions in the range of interest.

After the desired simulated flight conditions were stabilized, main burner lightoff was made at idle throttle setting from a windmill rotor speed of about 60 percent of rated speed. Four ports are provided at the compressor discharge station to allow high pressure air extraction for auxiliary aircraft systems. These ports were left open to increase compressor stall margin during engine acceleration from windmill. Once engine speed stabilized, these ports were closed for data acquisition.

The required rotor speed was then established at the minimum obtainable compressor pressure ratio. At the idle throttle setting, the minimum speed with the nozzle wide open was about 94 percent of rated speed. For speeds below about 94 percent the exhaust nozzle area was reduced while maintaining the idle throttle setting. For speeds above 94 percent, the throttle was advanced with the exhaust nozzle area full-open.

Each compressor stall point was approached along a line of constant corrected engine rotor speed. Incremental reductions of exhaust nozzle area were made, forcing the compressor to operate at higher compressor pressure ratios. Engine rotor speed was maintained at a constant value by manually biasing the throttle. Steady-state data were taken at each increment of nozzle area. Turbine discharge total temperature was monitored at each steady-state point and also at the stall point. Curves were drawn of compressor total-pressure ratio and corrected airflow as a function of the turbine discharge temperature reading. These curves were extrapolated to the turbine discharge temperature reading at the point of stall to determine compressor pressure ratio and corrected airflow at stall. In several instances compressor stall occurred after a steady-state reading, but before any reduction of exhaust nozzle area was made. Such instances required no extrapolation. In no case did the turbine discharge temperature at stall deviate from the immediately preceding steady-state reading by more than $50^{\circ}$ R (27.8 K).

## RESULTS AND DISCUSSION

### Clean Inlet Results

Compressor performance with undistorted inflow is presented in figure 3. The support grid structure was used in this test to effect a more valid comparison with the distorted inflow test results. The cusp in the stall line fairing at 90 percent corrected engine speed was probably related to the modified inlet guide vane-interstage bleed schedule used in this investigation (see the section Installation). At this speed, the inlet guide vanes were just full-open and the interstage bleed just full-closed. This tended to increase the loading of the front stages of the compressor, thereby reducing its stall margin. (See appendix B for definition of stall margin.) The stall line, the lines of constant corrected engine speed, and the standard engine normal operating line from this figure are reproduced in subsequent figures for ease of reference.

## Circumferential Distortion Patterns

The effect of 180° circumferential distortion on compressor performance is presented in figure 4. Figures 4(a) to (c) are listed in order of increasing screen mesh number or decreasing screen porosity. The porosity, in percent open area, was 57.4, 49.8, and 39.7 percent, respectively, for the $7\frac{1}{2}$, $8\frac{1}{2}$, and 9 screen mesh numbers. All these distortion levels had a serious effect on compressor pressure ratio at stall. Results indicate that the compressor pressure ratio at stall with distorted inflow decreased with increasing mesh number. There also appeared to be a tendency of the compressor to lose some corrected airflow pumping capacity with the higher mesh number screens, particularly at corrected engine speeds above 90 percent of rated speed. Only two stall points are presented in figure 4(c). This is because the compressor could not be stabilized at corrected engine speeds below about 92 percent with the compressor discharge ports closed (see the section Test Procedure).

The effect of 90° circumferential distortion on compressor performance is presented in figure 5. The stall line trends and compressor pumping characteristics obtained with the 90° pattern are very similar to those discussed for the 180° distortion pattern. In fact, for the same mesh screen, no significant difference between the 90° and the 180° distorted inflow stall lines was noted.

The effect of 60° circumferential distortion on compressor performance is presented in figure 6. Here again there appear to be no significant differences in performance between this and the 90° and 180° cases.

The effect of 30° circumferential spoiling on compressor performance is presented in figure 7. Only an $8\frac{1}{2}$ mesh number screen was tested with this pattern. Although serious, the effect of a 30° spoiled sector was not as deleterious to compressor performance as was the effect of the 60° or greater spoiled sectors of the same mesh number.

The effect of a circumferential distortion pattern using two diametrically opposed 60° screens of number $8\frac{1}{2}$ mesh was studied. Results are presented in figure 8. The compressor did not stall at 86.9 percent corrected engine speed because the required exhaust nozzle area was less than the minimum obtainable with the standard nozzle. The airflow blockage plates previously mentioned in the section Installation had not been installed for testing of this distortion pattern. If the results of figure 8 are compared to those presented in figure 6(b), it becomes apparent that stall margin degradation due to distorted inflow is less for cases of multiple spoiled sectors.

## Radial Distortion Patterns

The effect of hub radial distortion on compressor performance is presented in fig-

ure 9. Two mesh number screens were tested, each with spoiled areas of 20 and 40 percent of the total compressor face annulus area. The most obvious effect of hub radial distortion is a sizeable loss in the corrected airflow capacity of the compressor. Because compressor pressure ratio at stall did not fall off as fast as corrected engine airflow, there was little effect on overall compressor stall margin due to hub radial distortion. In fact, three of the four patterns tested showed a slight net increase in overall compressor stall margin over the speed range tested.

A midspan radial distortion pattern was tested using a $7\frac{1}{2}$ mesh number screen. Results are presented in figure 10. With the possible exception of the 100.0 percent corrected engine speed point, this type distortion showed no significant effect on compressor performance.

The effect of tip radial distortion on compressor performance is presented in figure 11. In contrast to hub radial, tip radial distortion had little effect on the corrected airflow capacity of the compressor. There was, however, a significant loss in compressor stall margin for those patterns with spoiled areas greater than 15 percent of the compressor face area. This loss was a direct function of the total pressure drop (or mesh number) of the screen. Increasing the spoiled area from 30 percent (figs. 11(b) and (d)) to 60 percent (figs. 11(c) and (e)) of the compressor face area seemed to have no additional effect on compressor performance.

The distortion pattern shown in figure 12 was run in order to determine what effect a reduction in spanwise pressure gradient would have on compressor performance. The innermost spoiled annulus of $7\frac{1}{2}$ mesh number screen was added to the tip radial screen pattern previously shown in figure 11(d). As expected from the results of figures 10 and 11, no significant effect of adding the inner screen was apparent.

## Combined Distortion Patterns

Tests were run on four combined screen patterns, each of which had both circumferential and radial distortion components. Results of the first of these are presented in figure 13. The pattern was a $120^{\circ}$ sector of the hub radial distortion screen previously shown in figure 9(e). In general, it appeared that the compressor was more sensitive to the circumferential component of distortion. Furthermore, the corrected airflow capacity of the compressor was not reduced as severely with the $120^{\circ}$ sector as it had been with the full $360^{\circ}$ radial pattern. As a result, compressor stall margin deterioration was far more serious than for the pure hub radial pattern.

Results of the second combined radial circumferential distortion pattern are presented in figure 14. This pattern was a $120^{\circ}$ sector of tip radial distortion made from number 9 mesh screen. Since no $360^{\circ}$ tip radial pattern was tested with a screen of this

mesh, the pattern closest in mesh number and radial extent was the $8\frac{1}{2}$ mesh $360^{\circ}$ screen shown in figure 11(d). Stall margin degradation for the $120^{\circ}$ sector is worse than for the pure radial case, but still not as bad as the $90^{\circ}$ circumferential pattern of figure 5(c). But because of the difference in screen mesh number between the pure tip radial and the combined pattern, no conclusion as to the greater sensitivity of the compressor to radial or circumferential distortion components can be drawn.

A $90^{\circ}$ circumferential distortion pattern ($8\frac{1}{2}$ mesh number) was tested in combination with a $270^{\circ}$ sector of hub radial ($7\frac{1}{2}$ mesh number). Results are presented in figure 15. The hub radial distortion pattern previously shown in figure 9(a) and the $90^{\circ}$ circumferential pattern shown in figure 5(b) can be used for comparison. Stall line deterioration for this combined pattern appears to be due primarily to the circumferential component of distortion. However, the deterioration was not as serious as it was for the pure circumferential distortion case. The decrease in corrected airflow capacity is attributed to the $270^{\circ}$ hub radial component.

Results of the fourth combined pattern are presented in figure 16. This pattern consisted of a $270^{\circ}$ sector of the tip radial pattern shown in figure 11(c) and the $90^{\circ}$ circumferential pattern shown in figure 5(a). Stall margin loss again appeared to be more closely related to the circumferential component of distortion. However, the $270^{\circ}$ radial component did have some effect since the stall line for the combined pattern fell below that of the pure circumferential pattern at corrected engine speeds below about 96 percent of rated speed.

## Distortion Indices

The compressor total pressure ratio at stall for undistorted inflow is presented in figure 17 as a function of corrected engine speed. In the compressor performance curves which follow, this pressure ratio is used to normalize the distorted inflow compressor pressure ratio at the same corrected engine speeds. Because no account is taken of variations in compressor corrected airflow, this parameter is not an ideal representation of compressor stall margin. However, its use provided a good correlation with a distortion index developed herein.

Most of the distortion indices now in use emphasize an area of below average pressure at the compressor face. In order to correlate a circumferential distortion index with compressor performance, however, some account must be taken of blade residence time in this low pressure area. The stall margin of the J85-GE-13 compressor has already been shown to be relatively insensitive to an increase in the included angle of spoiling (and, hence, blade residence time) beyond $60^{\circ}$ to $90^{\circ}$. This result is better illustrated in figure 18. The stall compressor pressure ratio is plotted as a function of cir-

cumferential extent of spoiling. Figures 18(a) to (c) pertain to screen mesh numbers of $7\frac{1}{2}$, $8\frac{1}{2}$, and 9, respectively. In each case, stall compressor pressure ratio fell rapidly as the spoiled angle was increased from $0^{\circ}$ to about $60^{\circ}$ and then stabilized at a nearly constant minimum value from $90^{\circ}$ to $180^{\circ}$. Hence, $60^{\circ}$ is the critical angle of distortion for the J85-GE-13 compressor. That is, it is the minimum angle of spoiling to which this compressor will respond in a quasi-steady-state manner.

Loss in stall compressor pressure ratio was plotted as a function of circumferential distortion indices. Results are presented in figure 19. Data shown in this figure include all of the stalls obtained with the individual $30^{\circ}$, $60^{\circ}$, $90^{\circ}$, and $180^{\circ}$ spoiled sectors. In figure 19(a), the extent of the spoiled sector was removed as a variable by plotting the ratio of minimum to maximum pressure rather than minimum to average pressure. Since the compressor has already been shown to be sensitive to a critical spoiling angle of about $60^{\circ}$, the $P_{min,60^{\circ}}$ used in this figure was defined as the lowest mean pressure in any $60^{\circ}$ sector of the compressor face flow field (see appendix C). By using this definition, the loss in stall compressor pressure ratio was correlated quite well to the level of pressure in the spoiled sector, regardless of circumferential extent. Because of some slight radial pressure gradients associated with surface boundary layers, the pressures discussed here were averaged radially.

In figure 19(b), these same data were plotted against a more commonly used distortion index, namely, $\left[1 - (P_{min,60^{\circ}}/\overline{P})\right]_2$. Since $\overline{P}$ is dependent upon circumferential extent, the single faired curve of figure 19(a) was transformed into the curves of figure 19(b) for constant extents of $60^{\circ}$, $90^{\circ}$, and $180^{\circ}$. The good correlation here demonstrates that this distortion index can be used with reasonable accuracy to predict loss in stall compressor pressure ratio if the extent of the low pressure region is known. The two stall points obtained with the multiple distortion pattern (two $60^{\circ}$ screens) are also plotted in figure 19(b). These points also correlated fairly well with the $60^{\circ}$ faired curve.

The $60^{\circ}$ and the $90^{\circ}$ curves of figure 19(b) can be practically collapsed into the $180^{\circ}$ curve by multiplying the distortion index by the square root of circumferential extent (in radians) divided by $\pi$. This is shown in figure 19(c). The single curve would be useful for programming a simple real-time dynamic distortion indicator.

An attempt to correlate results of the pure hub radial patterns shown in figure 9 and the pure tip radial patterns of figure 11 with a distortion index is presented in figures 20(a) and (b), respectively. The compressor face annulus was divided into five equal-area annular rings. Each ring centered on a probe of the five-tube total-pressure rakes. The $P_{min,r}$ used in this distortion index is the lowest mean pressure of any of the five rings. The compressor performance parameter, defined along the ordinate, is the same as that used in the circumferential distortion correlations. In figure 20(a), the deterioration of compressor performance at stall is seen to be a function of corrected engine speed. However, the parameter used to indicate compressor performance here

does not provide a true representation of the loss in compressor stall margin. From figure 9, it is readily seen that hub radial distortion can actually increase stall margin. In figure 20(b), the compressor performance parameter at stall is indicative of loss in stall margin, since tip radial distortion did not affect the pumping capacity of the compressor. All of the tip radial stalls obtained with spoiled extents of between 15 and 60 percent of the compressor face area are shown in this figure. The circumferential distortion correlation for a spoiled angle of $60^{\circ}$ is repeated here for reference. In general, the effects of tip radial distortion were not as severe as were those of an equal-area circumferential distortion.

Since hub radial distortion was shown to affect compressor pumping capacity rather than stall margin and since tip radial distortion was generally not found to be as serious as an equivalent circumferential distortion, it followed that a distortion index for a combined radial-circumferential pattern should accent the circumferential component. For analysis of data obtained with combined distortions, the compressor face annulus was divided into five equal-area rings as discussed in the previous paragraph. Then for each ring, the same circumferential distortion index defined in figure 19(b) for pure circumferential distortions was calculated. At stall, the loss in compressor pressure ratio was plotted against the maximum measured distortion index obtained for any of the five rings. Results are presented in figures 21 and 22.

Figure 21 pertains to the two $120^{\circ}$ sectors of pure radial distortion that were tested. The $120^{\circ}$ spoiled sector curve shown in this figure was obtained by a linear interpolation between the $90^{\circ}$ and the $180^{\circ}$ curves of figure 19(b). Compressor performance for those four points which fall significantly off the referenced curve (i.e., tip sectors at 93, 96, and 100 percent corrected engine speeds and hub sector at 100 percent corrected speed) was probably influenced by the radial component of the pattern. For these points, however, use of the circumferential distortion index in this manner results in a conservative estimate of loss in compressor performance.

Results of the two $270^{\circ}$ radial screen sectors combined with the $90^{\circ}$ circumferential distortion screens are presented in figure 22. These data generally showed excellent agreement with the $90^{\circ}$ curve for pure circumferential distortion, reproduced from figure 19(b). Except for the one stall point with a tip radial distortion component at a corrected engine speed of 100 percent, these results indicate that the circumferential component of a combined distortion pattern tends to predominate.

## SUMMARY OF RESULTS

An experimental investigation was made to determine the effect of steady-state total pressure distortion on a J85-GE-13 turbojet engine. Steady-state distortions were pro-

duced by placing screens approximately one engine diameter upstream of the compressor face. This program included varying the size and intensity of spoiled regions, both circumferential and radial. Some combined distortion patterns were studied. Results were used to develop a distortion index applicable to this engine regardless of the complexity of a pressure distortion presented it. The following results were obtained:

1. The compressor was found to be sensitive to a critical angle of $60^{\circ}$ of circumferential spoiling. At stall, the compressor total pressure ratio fell rapidly as the spoiled angle was increased from $0^{\circ}$ to about $60^{\circ}$, and then stabilized at a constant minimum value from $60^{\circ}$ to $180^{\circ}$. The critical angle is associated with a minimum blade residence time necessary to affect the compressor in a quasi-steady-state manner.

2. For pure circumferential distortions, the loss in compressor pressure ratio at stall was correlated to the level of pressure in the spoiled sector of the flow field. This pressure was defined as the lowest mean pressure in any $60^{\circ}$ sector of the flow field. Using this definition, a simple distortion index was identified as the deviation of the low pressure from average pressure ratioed to average pressure.

3. Hub radial distortion effected the corrected airflow pumping capacity and pressure ratio of the compressor, in a manner that did not significantly change compressor stall margin. Tip radial distortion did not effect the pumping capacity of the compressor, but rather the stall margin. However, loss in compressor pressure ratio at stall was generally not as great with tip radial distortion as it was for a circumferential distortion of the same intensity and extent. A graded tip radial pattern (two concentric screens of different porosities) was found to have about the same effect on the compressor as a single tip radial pattern of the lower porosity screen. A midspan radial distortion pattern was found to have no significant effect on compressor performance.

4. Deterioration of compressor performance when subjected to distortions with both radial and circumferential components was generally found to correlate with a circumferential distortion index.

5. A distortion pattern consisting of two diametrically opposed $60^{\circ}$ spoiled sectors was found to have a less serious effect on compressor performance than a single $60^{\circ}$ circumferential distortion pattern of the same intensity. The loss in compressor ratio at stall was found to correlate with the same distortion index used for a single $60^{\circ}$ distortion pattern.

Lewis Research Center,
National Aeronautics and Space Administration,
Cleveland, Ohio, November 10, 1970,
720-03.

## APPENDIX A

## SYMBOLS

| | |
|---|---|
| $A$ | area, $ft^2$ ($m^2$) |
| $A_{sp}$ | area of spoiled flow, $ft^2$ ($m^2$) |
| $A_2$ | compressor face annulus area, 1.284 $ft^2$ (0.1193 $m^2$) |
| $N$ | engine speed, rpm |
| $N^*$ | rated engine speed, 16 500 rpm |
| $(N/N^*\sqrt{\theta})\times 100$ | percent corrected engine speed |
| $P$ | total pressure, $lb/ft^2$ ($N/m^2$) |
| $P_{min,r}$ | minimum ring average pressure, $lb/ft^2$ ($N/m^2$) |
| $P_{min,60^o}$ | lowest mean pressure of any $60^o$ sector of compressor face flow field, $lb/ft^2$ ($N/m^2$) |
| ReI | Reynolds number index, $\delta_2/\varphi\sqrt{\theta_2}$ |
| $T$ | total temperature, $^oR$ (K) |
| $W$ | engine airflow, lb/sec (kg/sec) |
| $W_{corr}$ | engine corrected airflow, $W\sqrt{\theta}/\delta$, lb/sec (kg/sec) |
| $\beta$ | spoiled sector angle, deg |
| $\delta$ | local corrected total pressure, $P/2116$ $lb/ft^2$ ($P/101,325$ $N/m^2$) |
| $\theta$ | local corrected total temperature, $T/518.7^o$ R ($T/288.2$ K) |
| $\varphi$ | $(718.2^o \text{ R})\theta_2^{3/2}/(T_2 + 199.5^o \text{ R})$, $\left[(399 \text{ K})\theta_2^{3/2}/(T_2 + 110.8 \text{ K})\right]$ |

Subscripts:

| | |
|---|---|
| 1 | inlet airflow measuring station |
| 2 | compressor face measuring station |
| 3 | compressor discharge measuring station |
| 8 | nozzle throat station |
| max | maximum |
| min | minimum |
| r | any of the five equal annular areas (rings) of compressor face |

Superscripts:

| | |
|---|---|
| $\bar{}$ | average |

## APPENDIX B

## STALL MARGIN

Compressor stall margin is often defined as the difference between the compressor pressure ratios at stall and at the operating point divided by the compressor pressure ratio of the normal operating point. This difference is normally calculated along a constant corrected airflow line, as indicated by the following sketch:

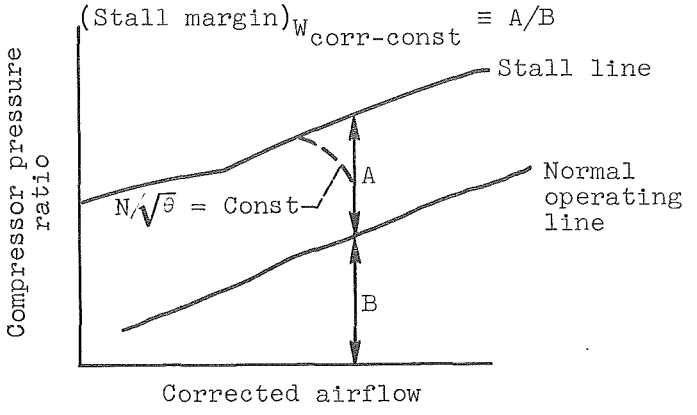


In this report stall margin is used only as a qualitative measure of the effects of total-pressure distortion on compressor performance. A loss in stall margin, then, would indicate that at a constant corrected airflow the compressor pressure ratio at stall for the distorted inflow case was less than the compressor pressure ratio for undistorted inflow at stall.

## APPENDIX C

## DEFINITION OF $P_{min, 60^o}$

$P_{min, 60^o}$ is defined as the lowest mean total pressure in any $60^o$ sector of the compressor face flow field; that is,

$$(P_{min, 60^o})_2 \equiv \frac{1}{60^o} \int_{\xi}^{\xi+60^o} P_2(\alpha)\, d\alpha \Bigg]_{\substack{\text{minimum value over range} \\ 0^o \leq \xi \leq 360^o}}$$

where

$60^o$ critical angle of spoiling for compressor

$\alpha$ angular displacement

$\xi$ dummy variable

An example of this definition for a square wave pressure distribution with a $30^o$ spoiled sector is shown in the following sketch:

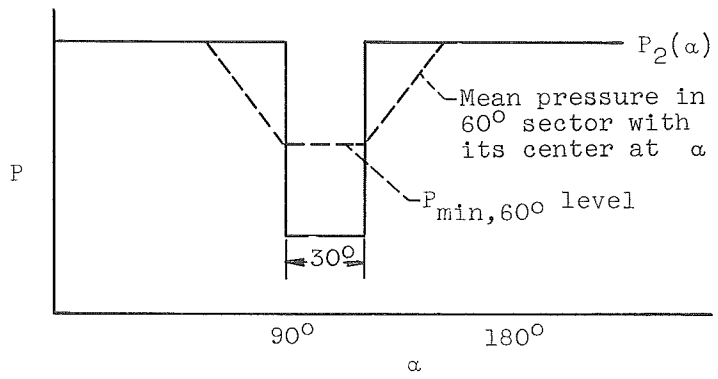

## REFERENCES


1. Pearson, H.; and McKenzie, A. B.: Wakes in Axial Compressors. J. Roy. Aeron. Soc., vol. 63, no. 583, July 1959, pp. 415-416.

2. Roberts, F.; Plourde, G. A.; and Smakula, F.: Insights into Axial Compressor Response to Distortion. Paper 68-565, AIAA, June 1968.

3. Reid, C.: The Response of Axial Flow Compressors to Intake Flow Distortion. Paper 69-GT-29, ASME, Mar. 1969.

4. Calogeras, James E.: Experimental Investigation of Dynamic Distortion in a Mach 2.50 Inlet with 60 Percent Internal Contraction and its Effect on Turbojet Stall Margin. NASA TM X-1842, 1969.

5. Coltrin, Robert E.; and Choby, David A.: Steady-State Interactions from Mach 1.98 to 2.58 Between a Turbojet Engine and an Axisymmetric Inlet With 60-Percent Internal Area Contraction. NASA TM X-1780, 1969.

6. McAulay, John E.: Effect of Dynamic Variations in Engine-Inlet Pressure on the Compressor System of a Twin-Spool Turbofan Engine. NASA TM X-2081, 1970.

7. Willoh, Ross G.; and Seldner, Kurt: Multistage Compressor Simulation Applied to the Prediction of Axial Flow Instabilities. NASA TM X-1880, 1969.

8. Antl, Robert J.; and Burley, Richard R.: Steady-State Airflow and Afterburning Performance Characteristics of Four J85-GE-13 Turbojet Engines. NASA TM X-1742, 1969.

TABLE I. - SCREEN PATTERNS

| Pattern | Type | Mesh | Wire diameter, in. (cm) | Porosity, percent open | Circumferential extent, deg | Spoiled area ratio, $A_{sp}$ $A_2$ | Percent corrected speed, $\frac{N}{N^*\sqrt{}} \cdot 100$ | Screen pressure drop, $\frac{P_{min.2}}{\bar{P}_1}$ | Distortion amplitude, $\left(\frac{P_{max} - P_{min}}{\bar{P}}\right)_2$ | Remarks |
|---|---|---|---|---|---|---|---|---|---|---|
| 1 | Circumferential | $7\frac{1}{2}$ | 0.032 (0.081) | 57.4 | 180 | 0.50 | 87.1 | 0.929 | 0.068 | Stall point |
| | | | | | | | 90.1 | .914 | .085 | |
| | | | | | | | 93.2 | .898 | .102 | |
| | | | | | | | 96.2 | .874 | .125 | |
| | | | | | | | 100.0 | .851 | .156 | |
| 2 | Circumferential | $8\frac{1}{2}$ | 0.035 (0.089) | 49.8 | 180 | 0.50 | 86.9 | 0.900 | 0.103 | Stall point |
| | | | | | | | 90.0 | .882 | .122 | |
| | | | | | | | 93.0 | .861 | .148 | |
| | | | | | | | 96.0 | .834 | .176 | |
| | | | | | | | 99.8 | .802 | .220 | |
| 3 | Circumferential | 9 | 0.041 (0.104) | 39.7 | 180 | 0.50 | 93.0 | 0.808 | 0.196 | Stall point |
| | | | | | | | 100.1 | .745 | .274 | Stall point |
| 4 | Circumferential | $7\frac{1}{2}$ | 0.032 (0.081) | 57.4 | 90 | 0.25 | 87.0 | 0.932 | 0.066 | Stall point |
| | | | | | | | 93.0 | .905 | .091 | |
| | | | | | | | 100.0 | .864 | .126 | |
| 5 | Circumferential | $8\frac{1}{2}$ | 0.035 (0.089) | 49.8 | 90 | 0.25 | 87.0 | 0.918 | 0.080 | Stall point |
| | | | | | | | 89.9 | .900 | .097 | |
| | | | | | | | 92.9 | .885 | .112 | |
| | | | | | | | 95.9 | .866 | .129 | |
| | | | | | | | 99.7 | .840 | .159 | |
| 6 | Circumferential | 9 | 0.041 (0.104) | 39.7 | 90 | 0.25 | 92.9 | 0.849 | 0.154 | Stall point |
| | | | | | | | 100.0 | .792 | .215 | Stall point |
| 7 | Circumferential | $7\frac{1}{2}$ | 0.032 (0.081) | 57.4 | 60 | 0.167 | 86.9 | 0.937 | 0.058 | Stall point |
| | | | | | | | 89.9 | .984 | .069 | |
| | | | | | | | 92.9 | .912 | .080 | |
| | | | | | | | 96.0 | .895 | .095 | |
| | | | | | | | 99.9 | .870 | .113 | |
| 8 | Circumferential | $8\frac{1}{2}$ | 0.035 (0.089) | 49.8 | 60 | 0.167 | 86.7 | 0.922 | 0.070 | Stall point |
| | | | | | | | 89.9 | .910 | .086 | |
| | | | | | | | 92.8 | .894 | .097 | |
| | | | | | | | 96.1 | .872 | .118 | |
| | | | | | | | 99.7 | .848 | .138 | |
| 9 | Circumferential | 9 | 0.041 (0.104) | 39.7 | 60 | 0.167 | 87.3 | 0.900 | 0.094 | Stall point |
| | | | | | | | 92.9 | .863 | .133 | |
| | | | | | | | 99.8 | .806 | .189 | |
| 10 | Circumferential | $8\frac{1}{2}$ | 0.035 (0.089) | 49.8 | 30 | 0.083 | 87.0 | 0.937 | 0.078 | Stall point |
| | | | | | | | 90.1 | .923 | .095 | |
| | | | | | | | 93.2 | .907 | .114 | |
| | | | | | | | 96.2 | .890 | .135 | |
| | | | | | | | 100.3 | .868 | .161 | |
| 11 | Circumferential (dual sectors) | $8\frac{1}{2}$ | 0.035 (0.089) | 49.8 | 60 | 0.333 | 86.9 | 0.913 | 0.081 | Minimum $A_{sp}$; no stall |
| | | | | | | | 93.0 | .880 | .110 | Stall point |
| | | | | | | | 99.7 | .822 | .171 | Stall point |
| 12 | Hub radial | $7\frac{1}{2}$ | 0.032 (0.081) | 57.4 | 360 | 0.20 | 87.0 | 0.942 | 0.055 | Stall point |
| | | | | | | | 92.9 | .920 | .076 | |
| | | | | | | | 99.9 | .869 | .126 | |
| 13 | Hub radial | $7\frac{1}{2}$ | 0.032 (0.081) | 57.4 | 360 | 0.40 | 86.9 | 0.940 | 0.055 | Stall point |
| | | | | | | | 92.9 | .913 | .080 | |
| | | | | | | | 99.9 | .861 | .130 | |

TABLE I. - Concluded. SCREEN PATTERNS

| Pattern | Type | Mesh | Wire diameter, in. (cm) | Porosity, percent open | Circumferential extent, deg | Spoiled area ratio, $A_{sp}/A_2$ | Percent corrected speed, $\frac{N}{N\cdot\sqrt{\theta}}\cdot 100$ | Screen pressure drop, $\frac{P_{min,2}}{\bar{P}_1}$ | Distortion amplitude, $\left(\frac{P_{max}-P_{min}}{\bar{P}}\right)_2$ | Remarks |
|---|---|---|---|---|---|---|---|---|---|---|
| 14 | Hub radial | 9 | 0.041 (0.104) | 39.7 | 360 | 0.20 | 87.1 | 0.909 | 0.087 | Stall point |
| | | | | | | | 90.2 | .895 | .100 | |
| | | | | | | | 93.0 | .876 | .118 | |
| | | | | | | | 96.0 | .852 | .151 | |
| | | | | | | | 99.9 | .810 | .189 | |
| 15 | Hub radial | 9 | 0.041 (0.104) | 39.7 | 360 | 0.40 | 87.4 | 0.887 | 0.110 | Minimum $A_8$; no stall |
| | | | | | | | 90.2 | .875 | .123 | |
| | | | | | | | 93.5 | .853 | .146 | |
| | | | | | | | 96.0 | .830 | .172 | |
| | | | | | | | 100.1 | .777 | .233 | |
| 16 | Midspan radial | $7\frac{1}{2}$ | 0.032 (0.081) | 57.4 | 360 | 0.40 | 86.9 | 0.934 | 0.055 | Stall point |
| | | | | | | | 89.8 | .922 | .065 | |
| | | | | | | | 92.9 | .908 | .078 | |
| | | | | | | | 95.9 | .882 | .099 | |
| | | | | | | | 100.0 | .858 | .126 | |
| 17 | Tip radial | $7\frac{1}{2}$ | 0.032 (0.081) | 57.4 | 360 | 0.15 | 87.1 | 0.943 | 0.053 | Stall point |
| | | | | | | | 90.2 | .935 | .060 | |
| | | | | | | | 93.0 | .924 | .070 | |
| | | | | | | | 96.1 | .908 | .084 | |
| | | | | | | | 100.1 | .888 | .098 | |
| 18 | Tip radial | $7\frac{1}{2}$ | 0.032 (0.081) | 57.4 | 360 | 0.30 | 92.9 | 0.906 | 0.088 | Stall point |
| | | | | | | | 95.8 | .887 | .107 | |
| | | | | | | | 99.8 | .865 | .127 | |
| 19 | Tip radial | $7\frac{1}{2}$ | 0.032 (0.081) | 57.4 | 360 | 0.60 | 87.0 | 0.921 | 0.073 | Stall point |
| | | | | | | | 98.8 | .907 | .087 | |
| | | | | | | | 92.8 | .895 | .096 | |
| | | | | | | | 95.7 | .873 | .114 | |
| | | | | | | | 99.6 | .848 | .141 | |
| 20 | Tip radial | $8\frac{1}{2}$ | 0.035 (0.089) | 49.8 | 360 | 0.30 | 92.9 | 0.883 | 0.115 | Stall point |
| | | | | | | | 99.9 | .837 | .170 | Stall point |
| 21 | Tip radial | $8\frac{1}{2}$ | 0.035 (0.089) | 49.8 | 360 | 0.60 | 87.1 | 0.889 | 0.107 | Stall point |
| | | | | | | | 93.0 | .850 | .148 | |
| | | | | | | | 100.0 | .797 | .207 | |
| 22 | Graded tip radial | $8\frac{1}{2}$ (Outer ring) | 0.035 (0.089) | 49.8 | 360 | 0.30 | 87.1 | 0.893 | 0.106 | Stall point |
| | | | | | | | 93.1 | .862 | .137 | |
| | | $7\frac{1}{2}$ (Inner ring) | 0.032 (0.081) | 57.4 | 360 | 0.30 | 96.0 | .834 | .170 | |
| | | | | | | | 99.9 | .811 | .195 | |
| 23 | Hub radial sector | 9 | 0.041 (0.104) | 39.7 | 120 | 0.067 | 87.1 | 0.912 | 0.080 | Stall point |
| | | | | | | | 90.0 | .897 | .095 | |
| | | | | | | | 93.0 | .881 | .109 | |
| | | | | | | | 96.1 | .857 | .132 | |
| | | | | | | | 100.0 | .825 | .161 | |
| 24 | Tip radial sector | 9 | 0.041 (0.104) | 39.7 | 120 | 0.133 | 87.1 | 0.903 | 0.095 | Stall point |
| | | | | | | | 90.0 | .886 | .111 | |
| | | | | | | | 92.9 | .869 | .131 | |
| | | | | | | | 96.0 | .844 | .158 | |
| | | | | | | | 99.9 | .817 | .186 | |
| 25 | Combined radial and circumferential | $7\frac{1}{2}$ (Hub radial) | 0.032 (0.081) | 57.4 | 270 | 0.15 | 87.0 | 0.818 | 0.076 | Stall point |
| | | | | | | | 93.0 | .887 | .107 | |
| | | $8\frac{1}{2}$ (Circumferential) | 0.035 (0.089) | 49.8 | 90 | .25 | 100.0 | .832 | .162 | |
| 26 | Combined radial and circumferential | $7\frac{1}{2}$ (Tip radial) | 0.032 (0.081) | 57.4 | 270 | 0.45 | 87.0 | 0.920 | 0.084 | Stall point |
| | | | | | | | 93.0 | .887 | .124 | |
| | | $8\frac{1}{2}$ (Circumferential | 0.032 (0.081) | 57.4 | 90 | .25 | 100.0 | .845 | .166 | |

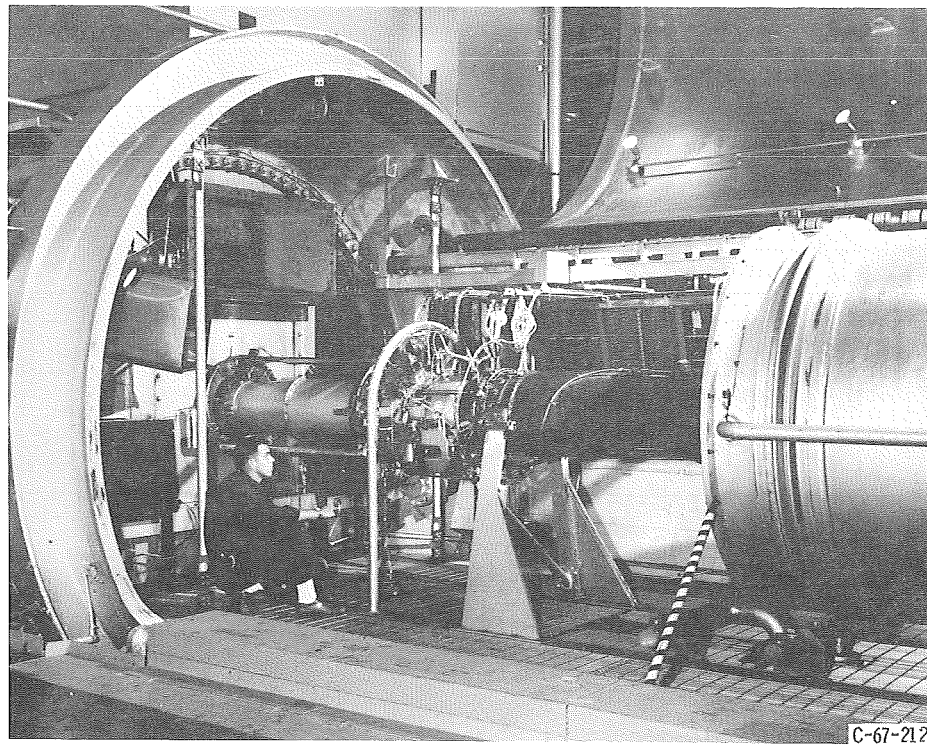


(a) Turbojet engine (J85-GE-13) installed in altitude chamber.

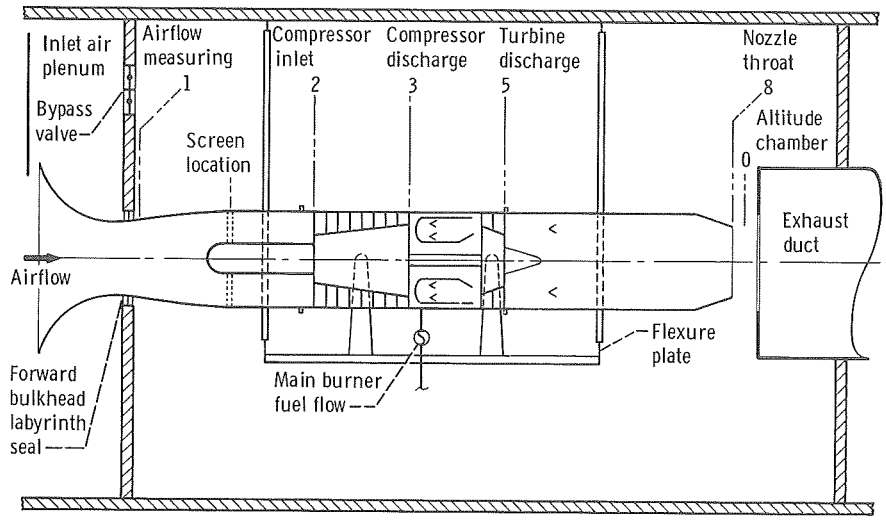


(b) Schematic showing measuring stations.

CD-10152-28

Figure 1. - Test installation.

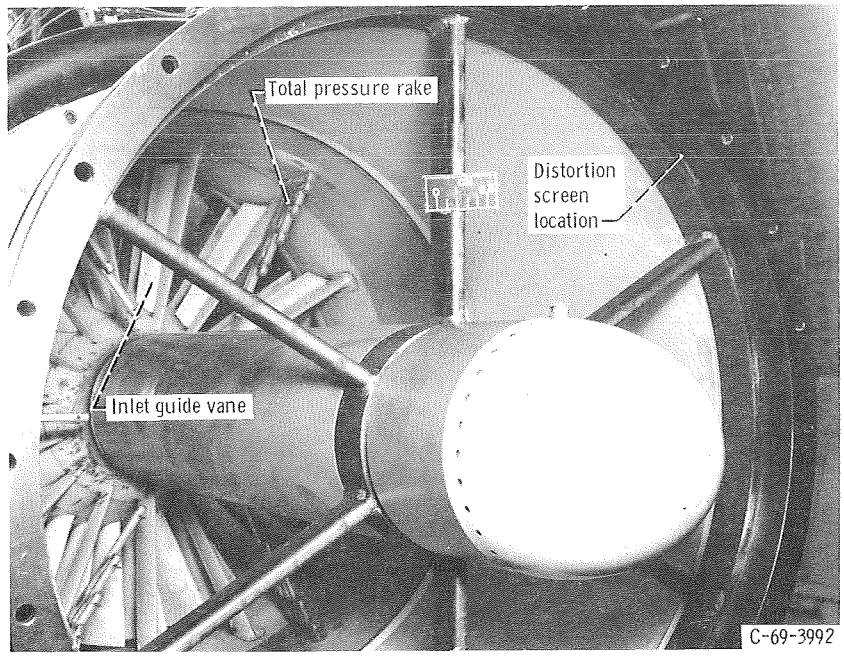


(c) Bullet-nose extension.

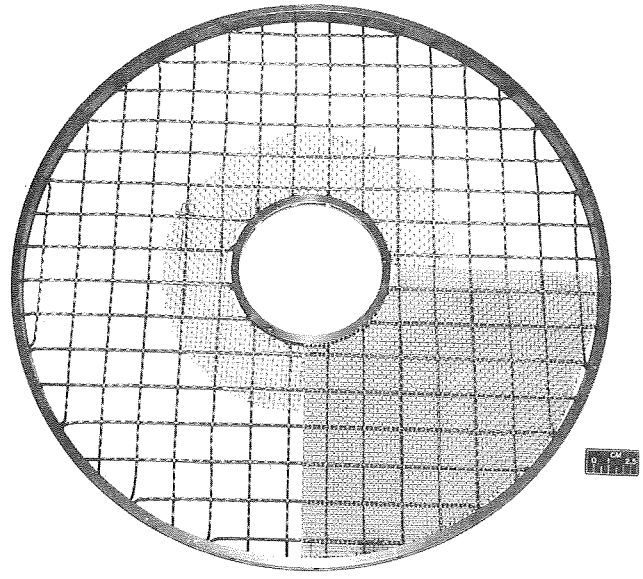


(d) Screen pattern number 25 mounted on support grid.

Figure 1. - Concluded.

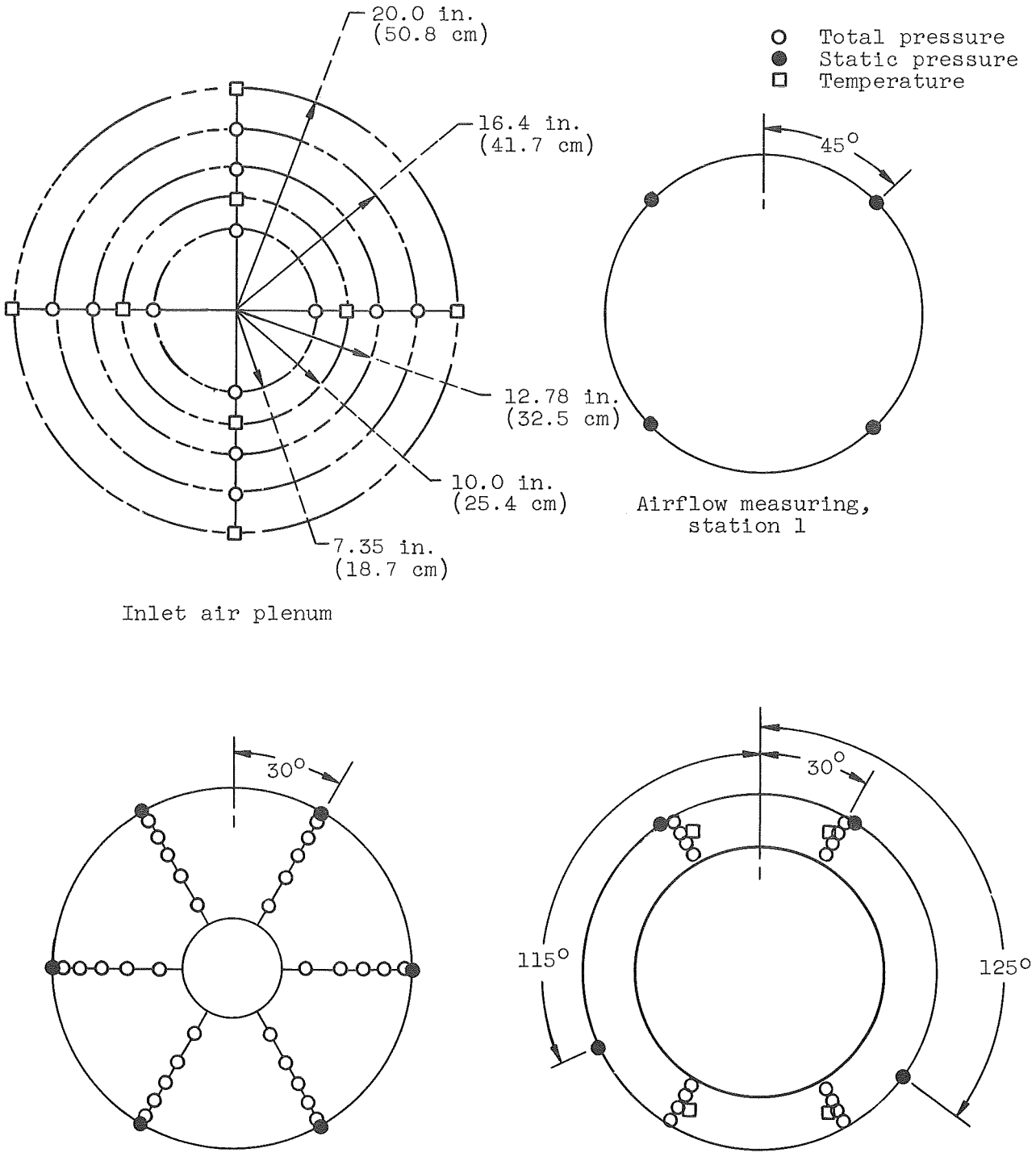


Figure 2. - Instrumentation schematic as viewed from upstream.

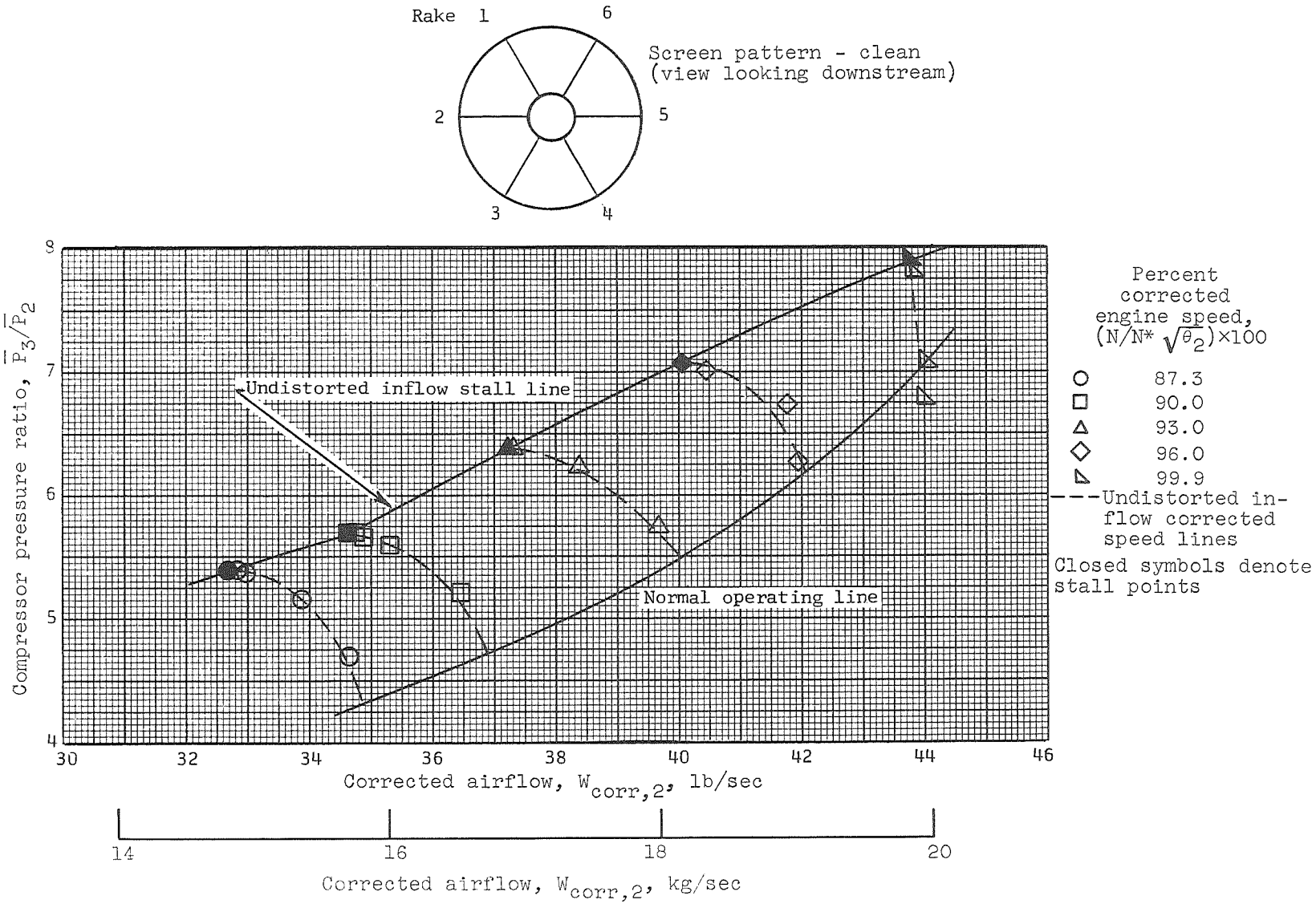


Figure 3. - Compressor performance with undistorted inflow.

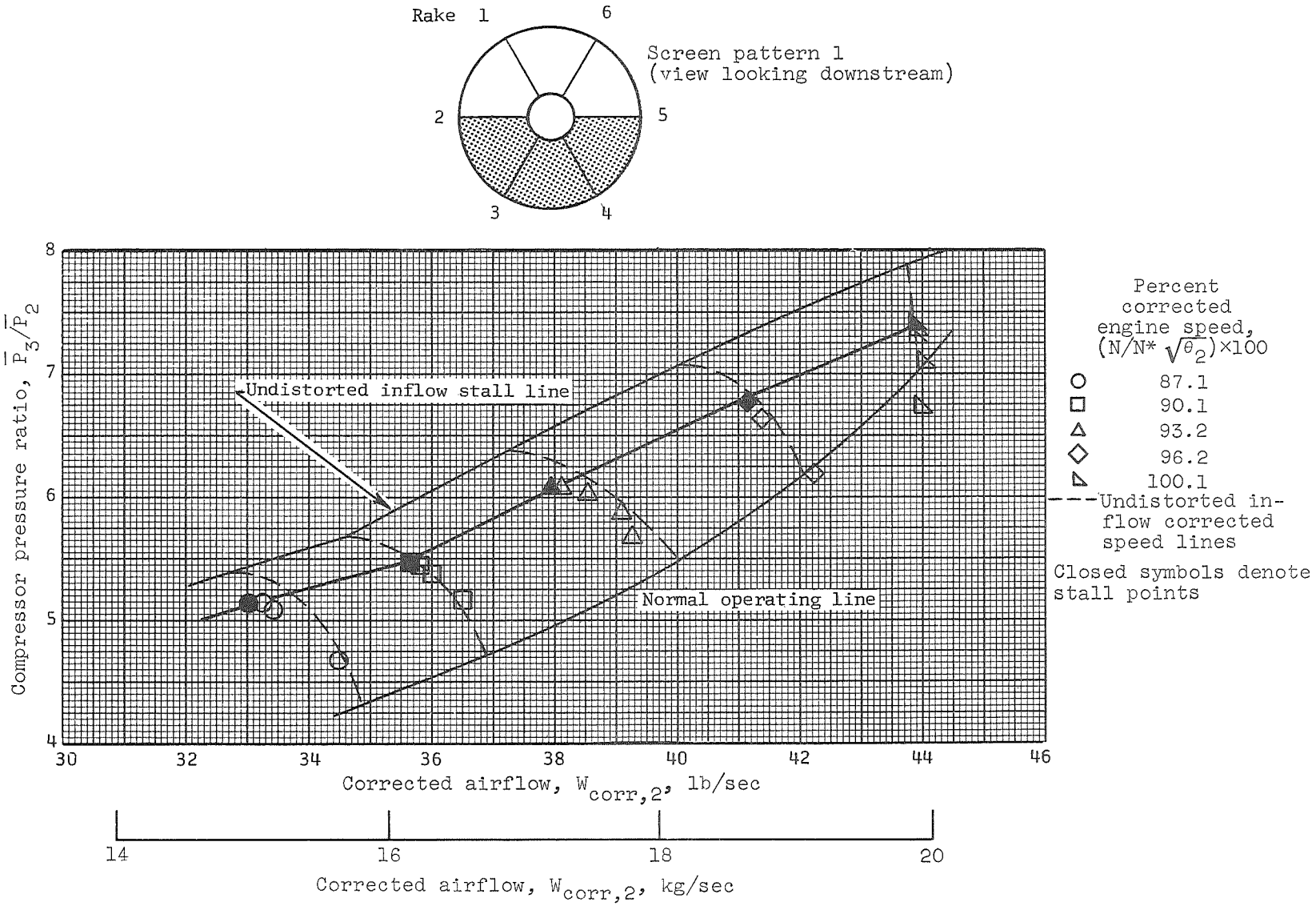


(a) $7\frac{1}{2}$ mesh screen.

Figure 4. - Compressor performance with 180° circumferential distortion.

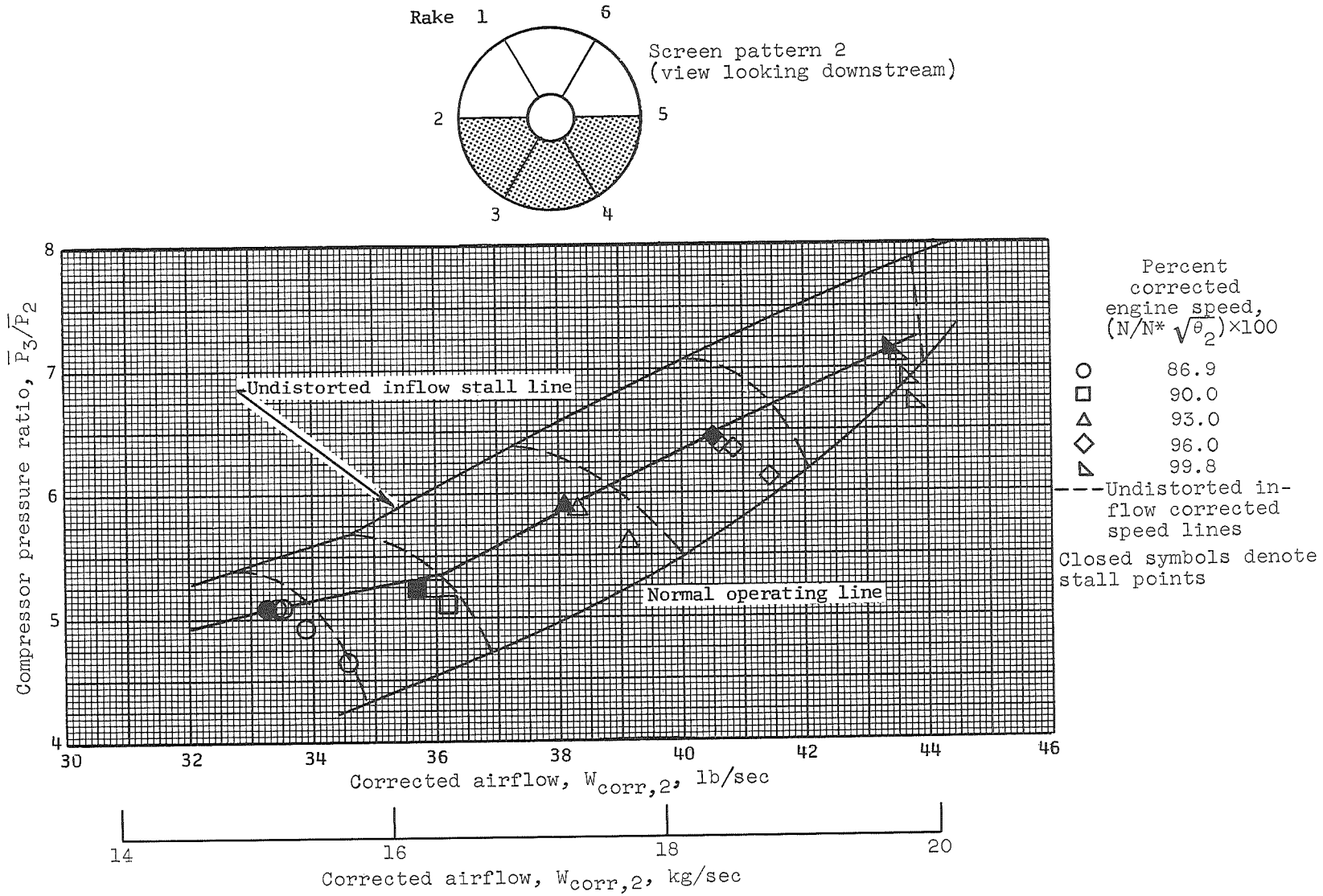


(b) $8\frac{1}{2}$ mesh screen.

Figure 4. - Continued.

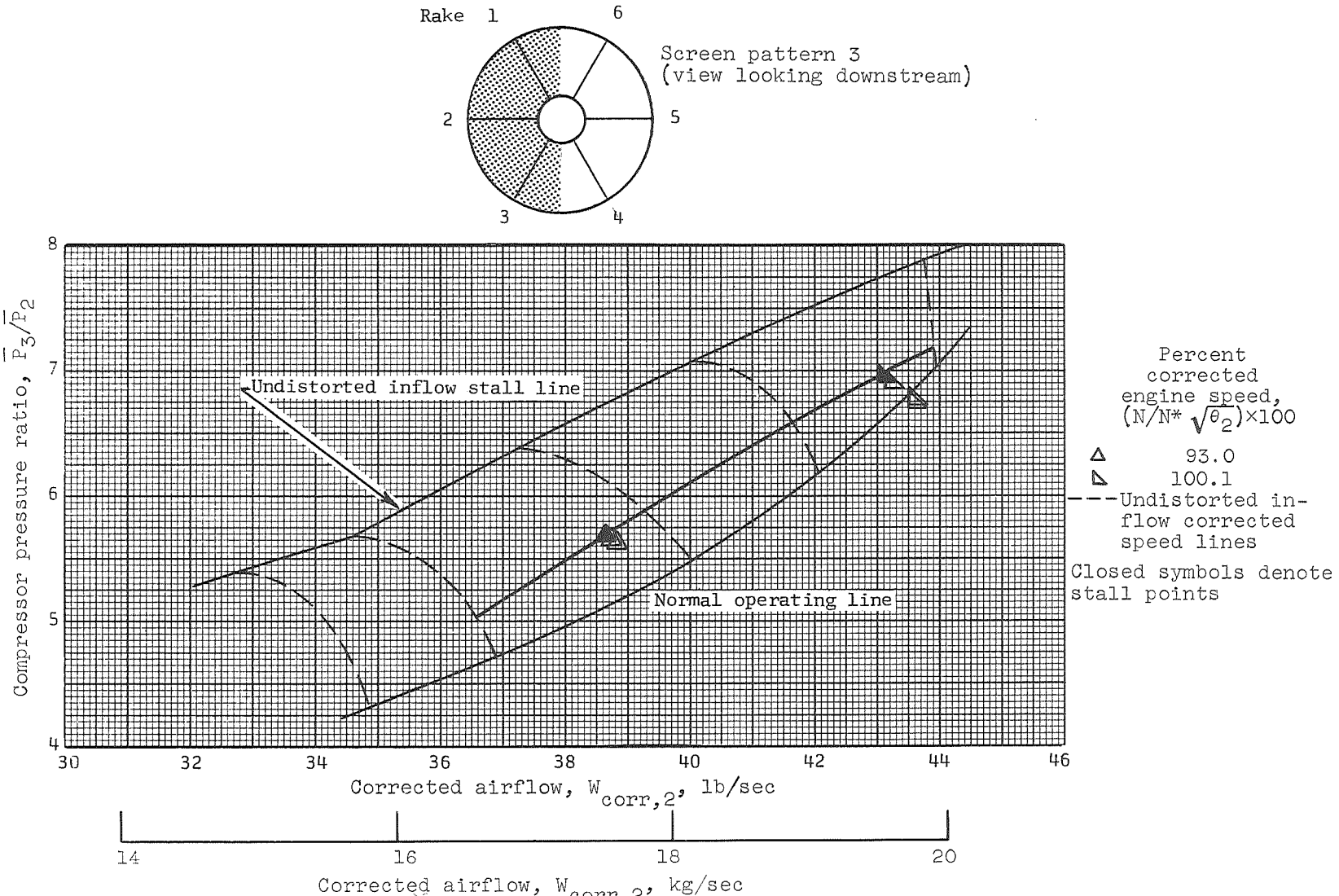


(c) 9 mesh screen.

Figure 4. - Concluded.

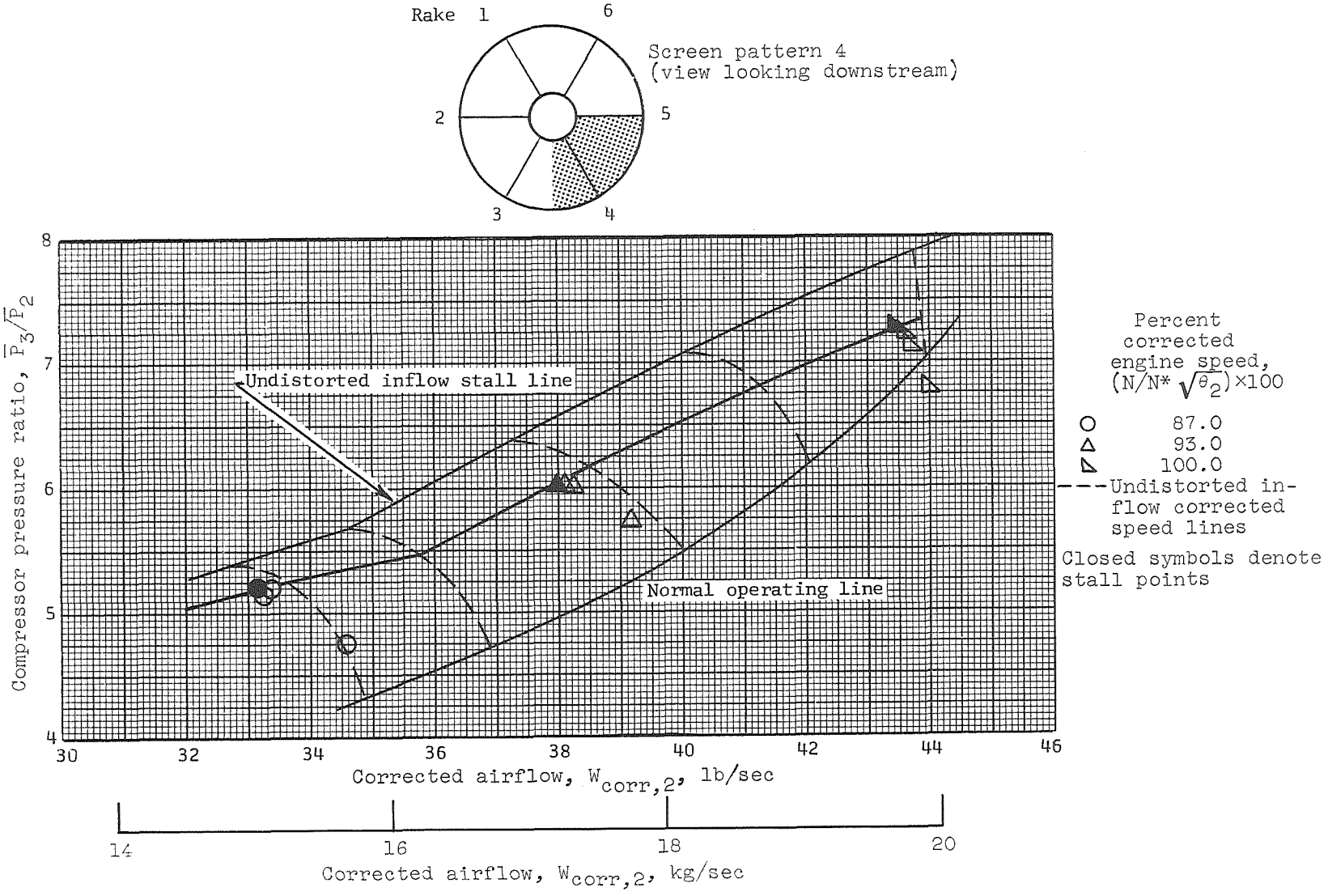


(a) $7\frac{1}{2}$ mesh screen.

Figure 5. - Compressor performance with 90° circumferential distortion.

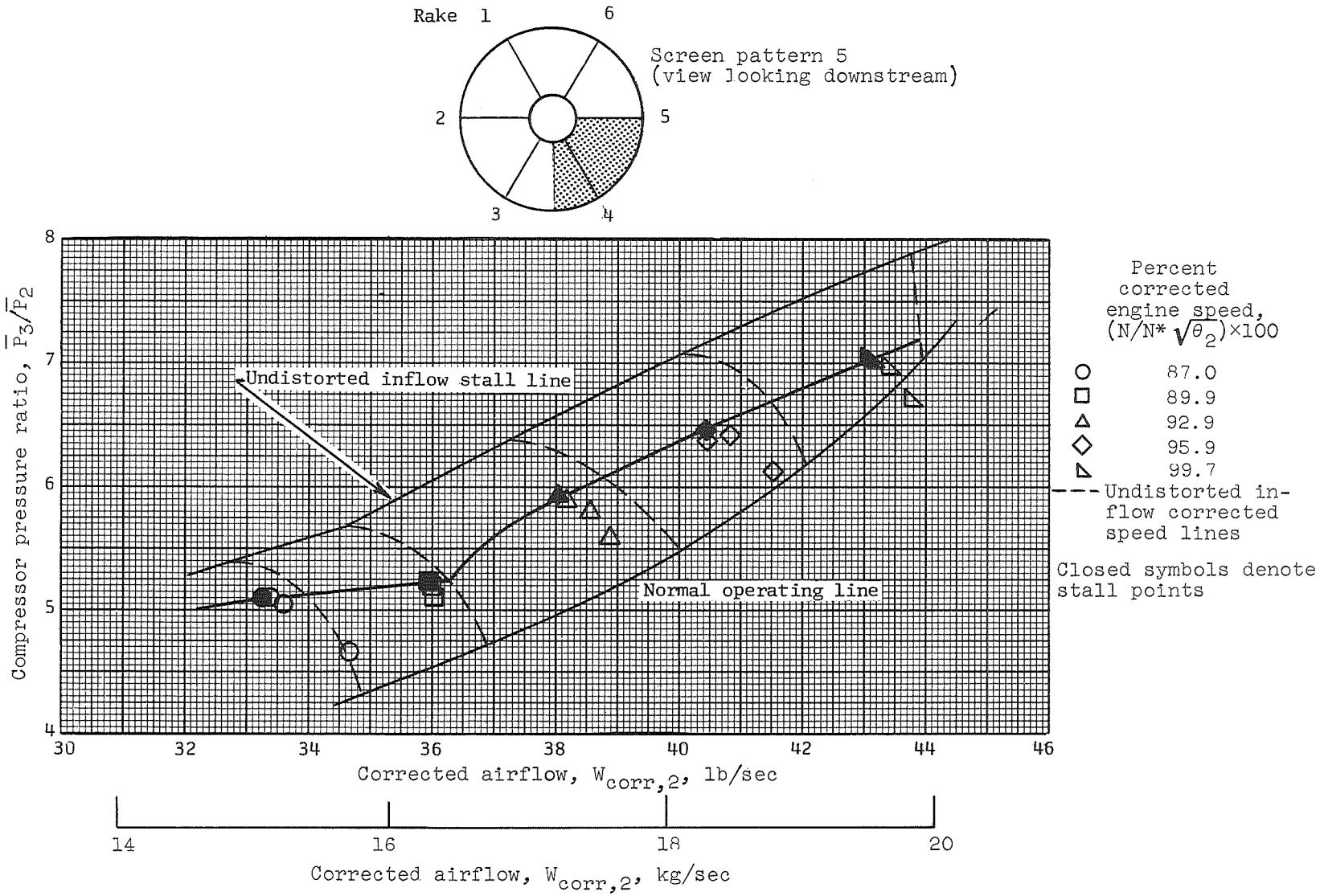


(b) $8\frac{1}{2}$ mesh screen.

Figure 5. - Continued.

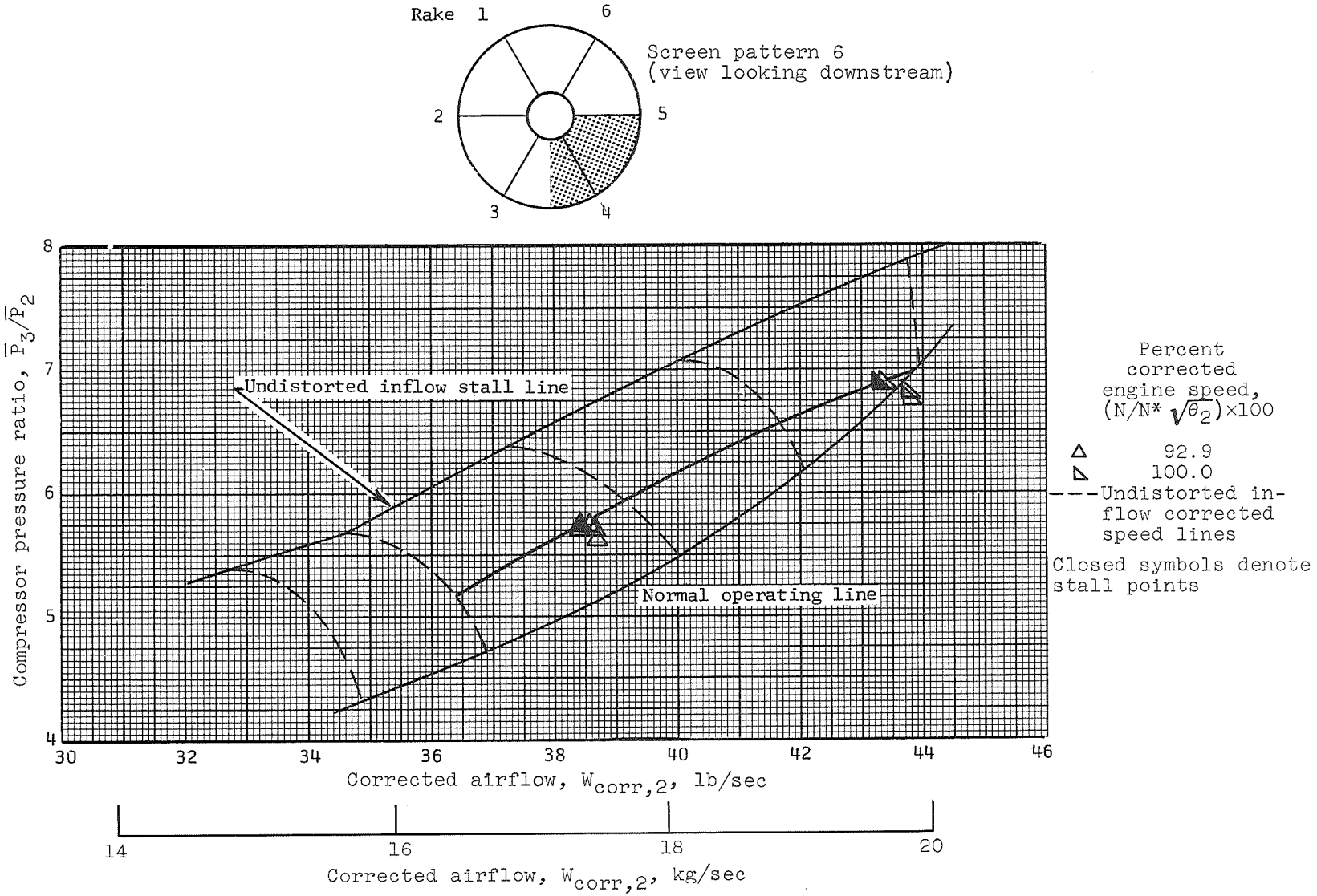


(c) 9 mesh screen.

Figure 5. - Concluded.

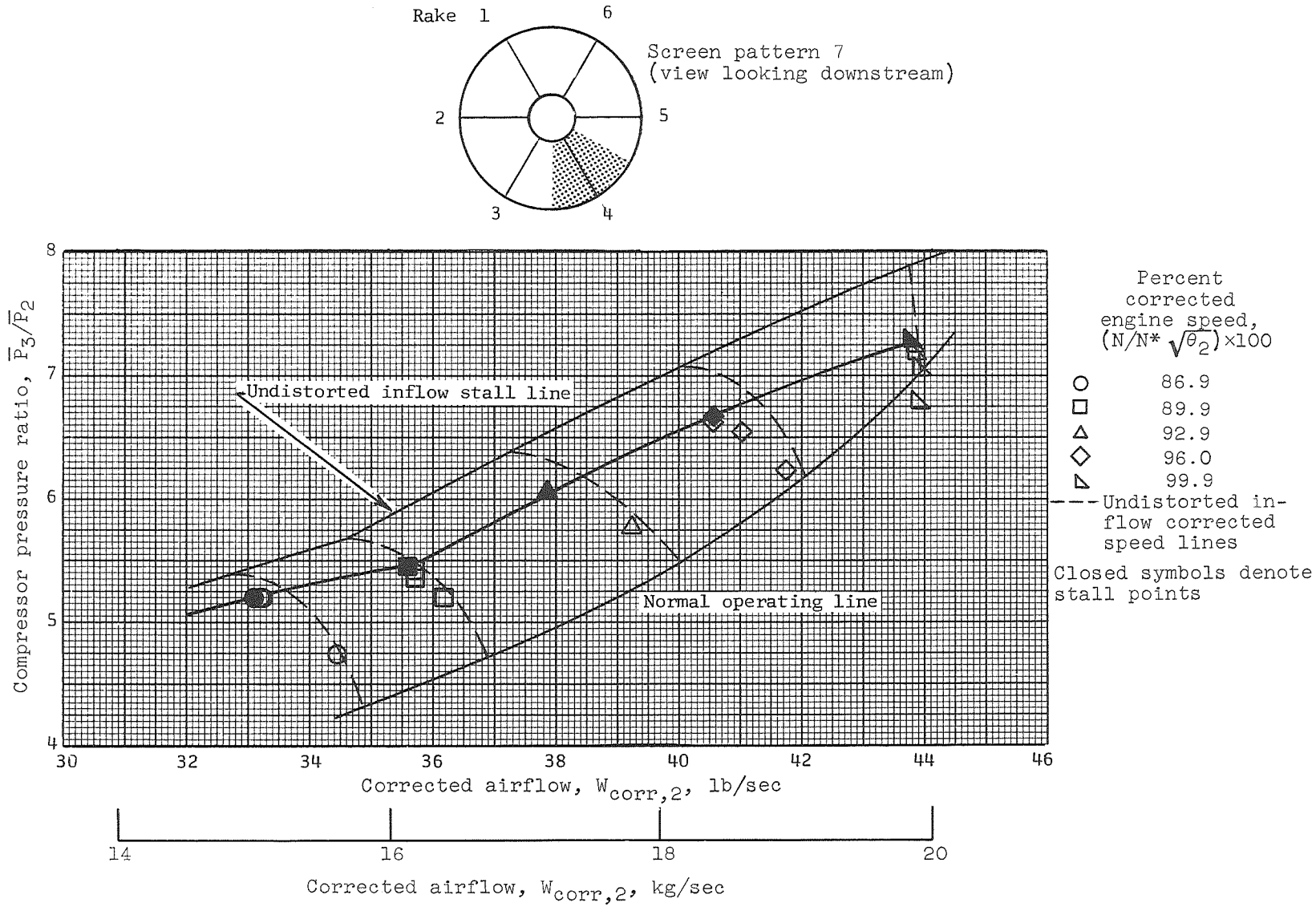


(a) $7\frac{1}{2}$ mesh screen.

Figure 6. - Compressor performance with 60° circumferential distortion.

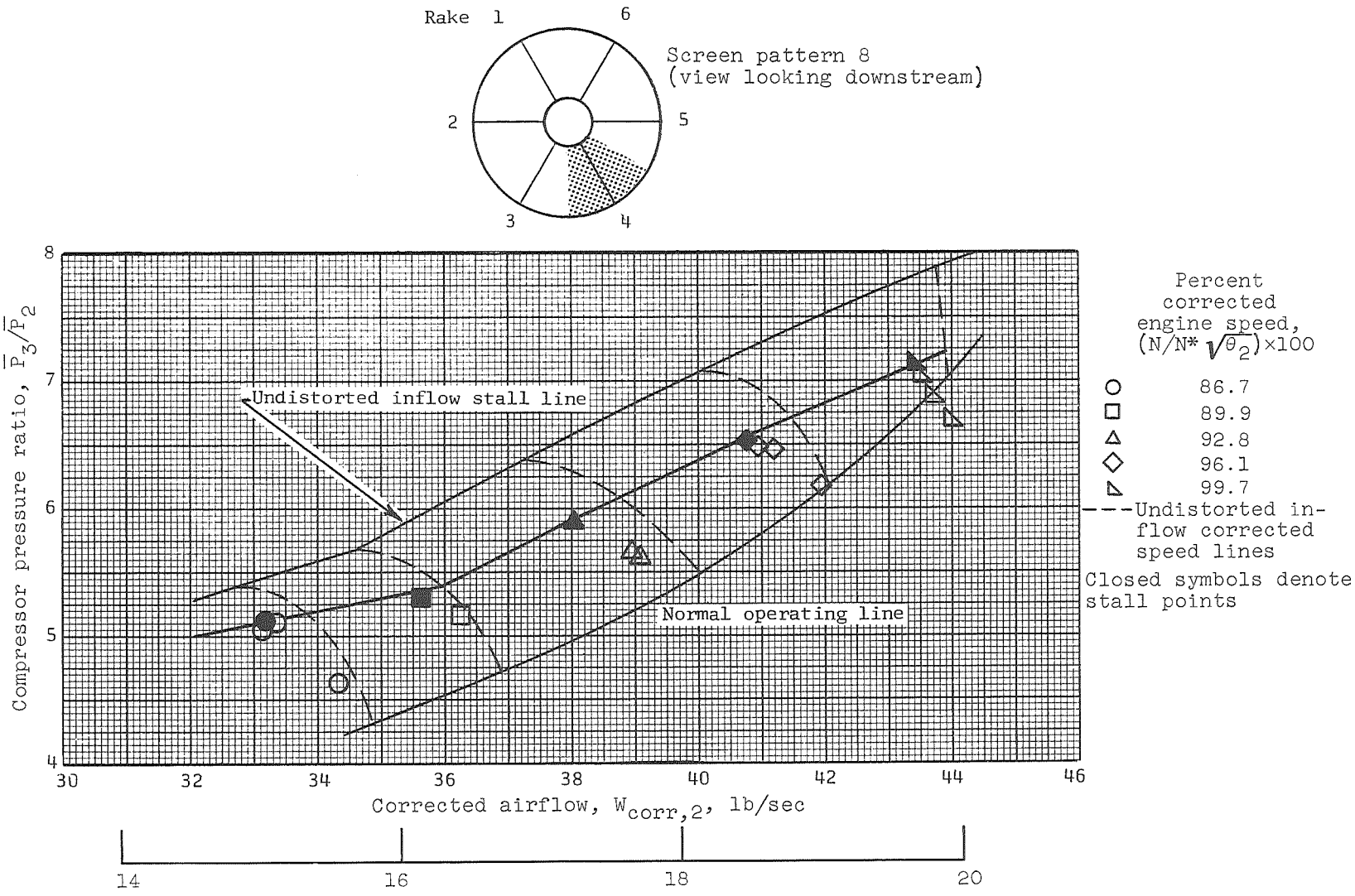


(b) $8\frac{1}{2}$ mesh screen.

Figure 6. - Continued.

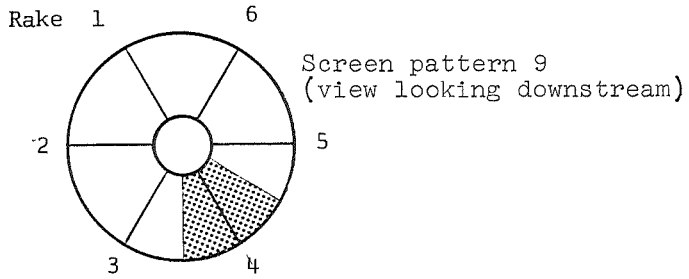


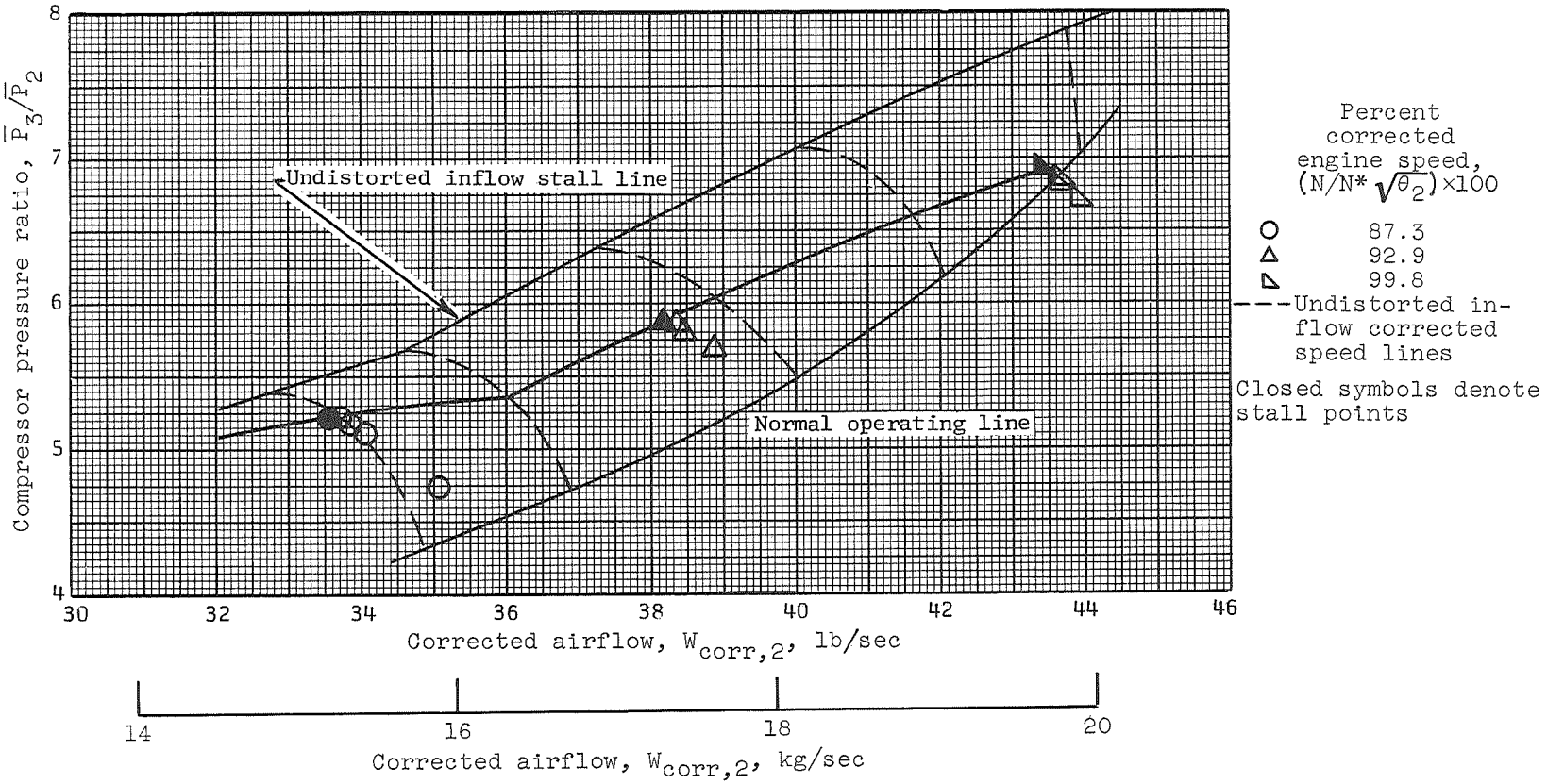


(c) 9 mesh screen.

Figure 6. - Concluded.

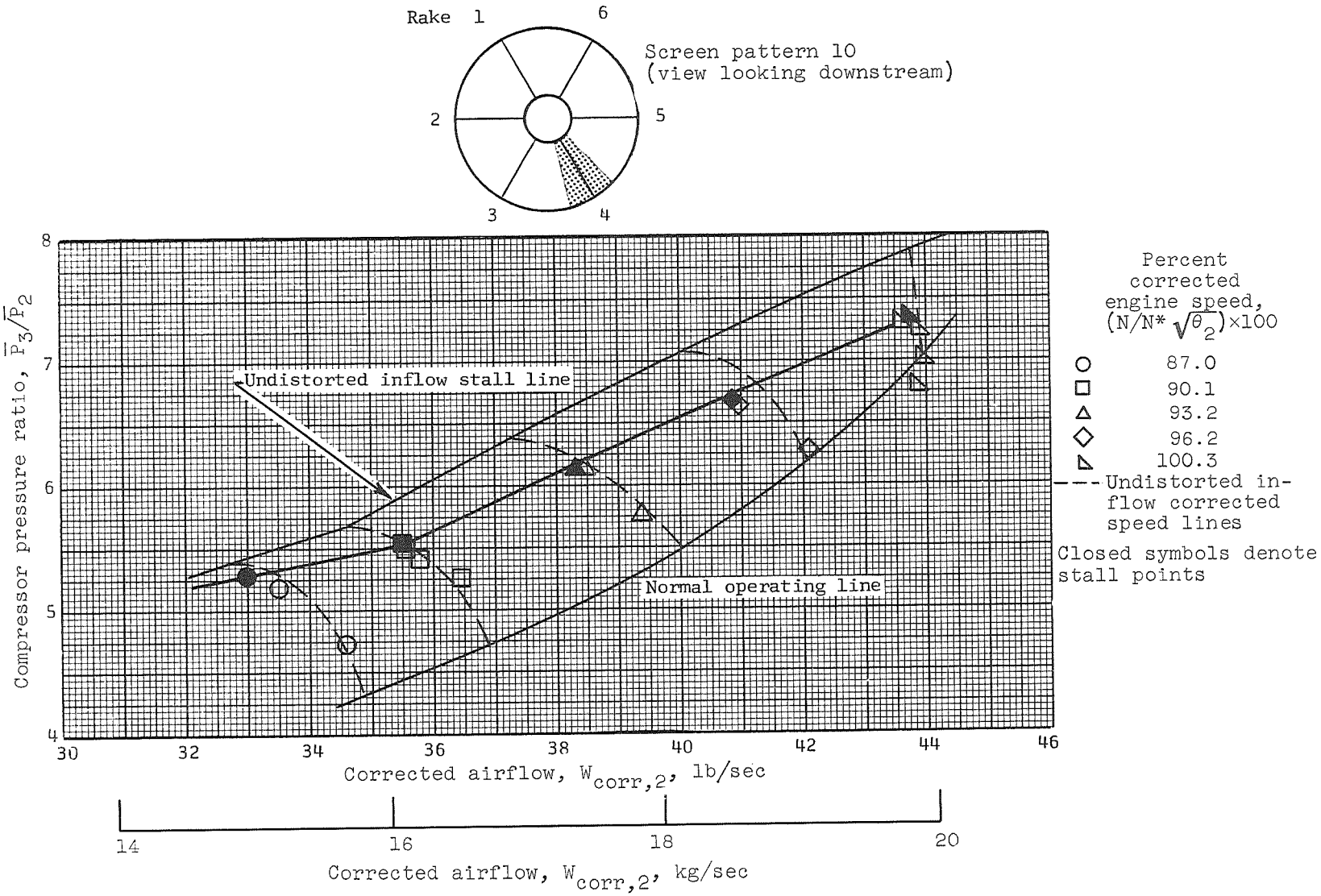


Figure 7. - Compressor performance with 30° circumferential distortion; $8\frac{1}{2}$ mesh screen.

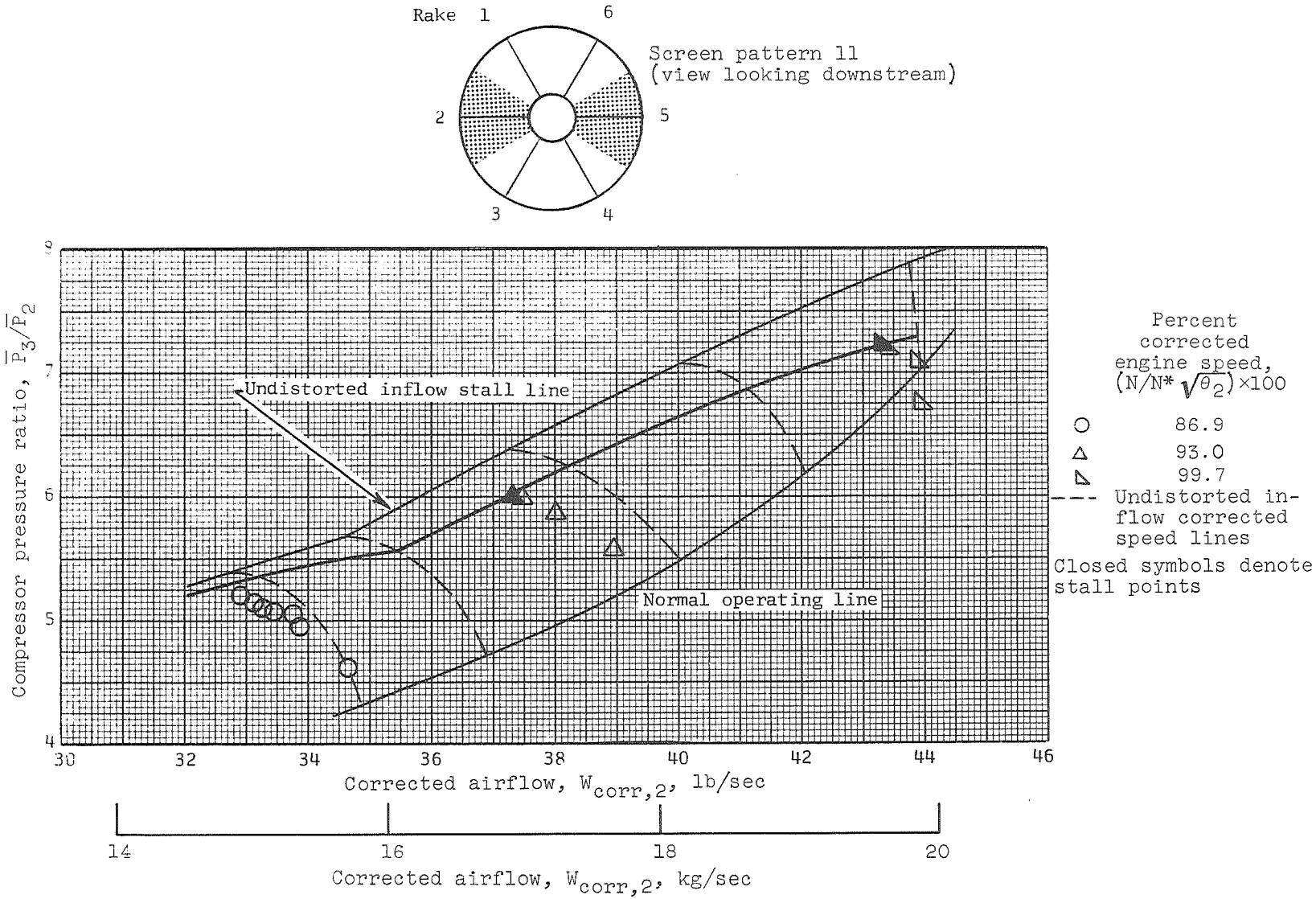


Figure 8. - Compressor performance with two diametrically opposite 60° circumferential distortion screens of $8\frac{1}{2}$ mesh.

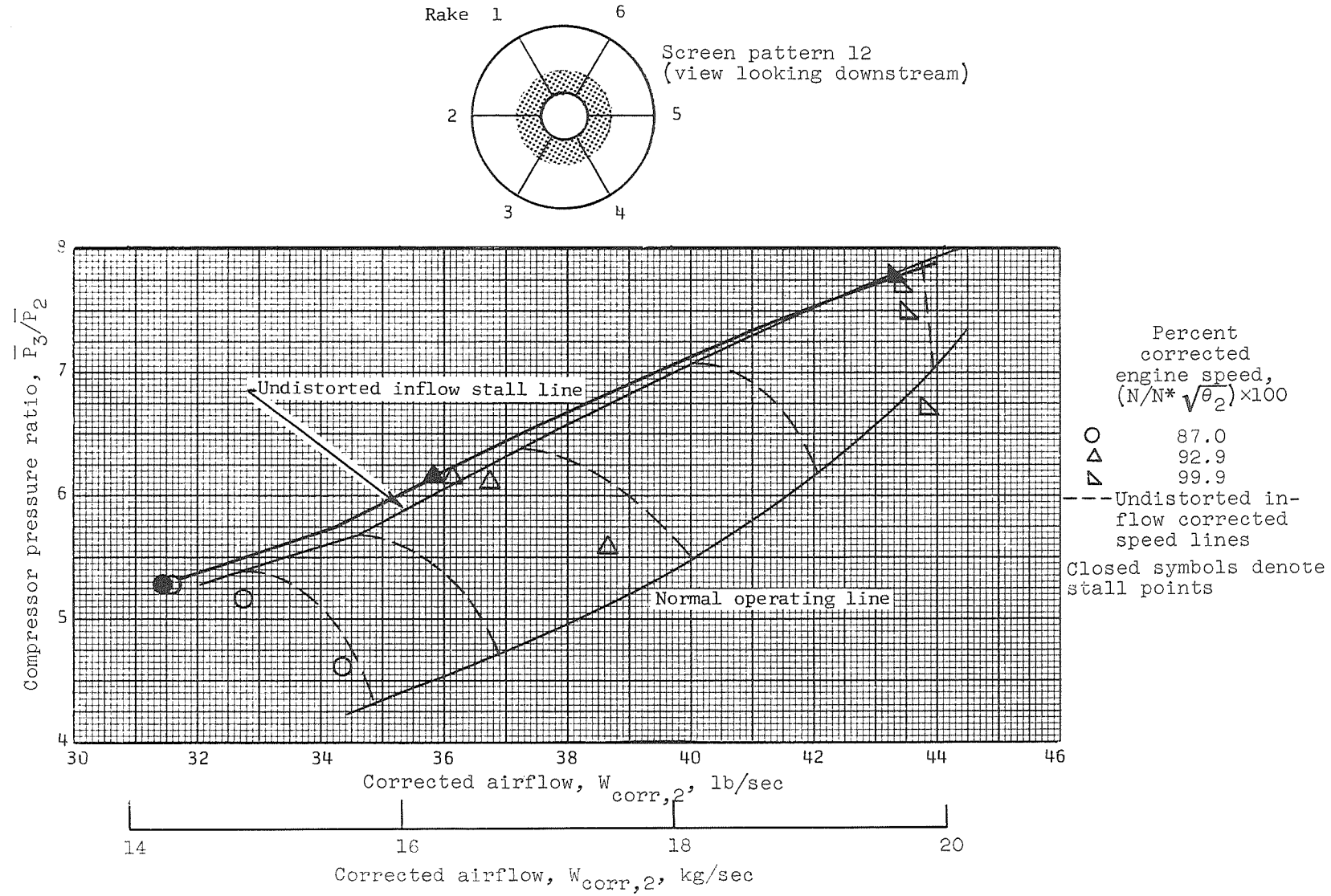


(a) $7\frac{1}{2}$ mesh screen; $A_{sp}/A_2 = 0.2$.

Figure 9. - Compressor performance with hub radial distortion.

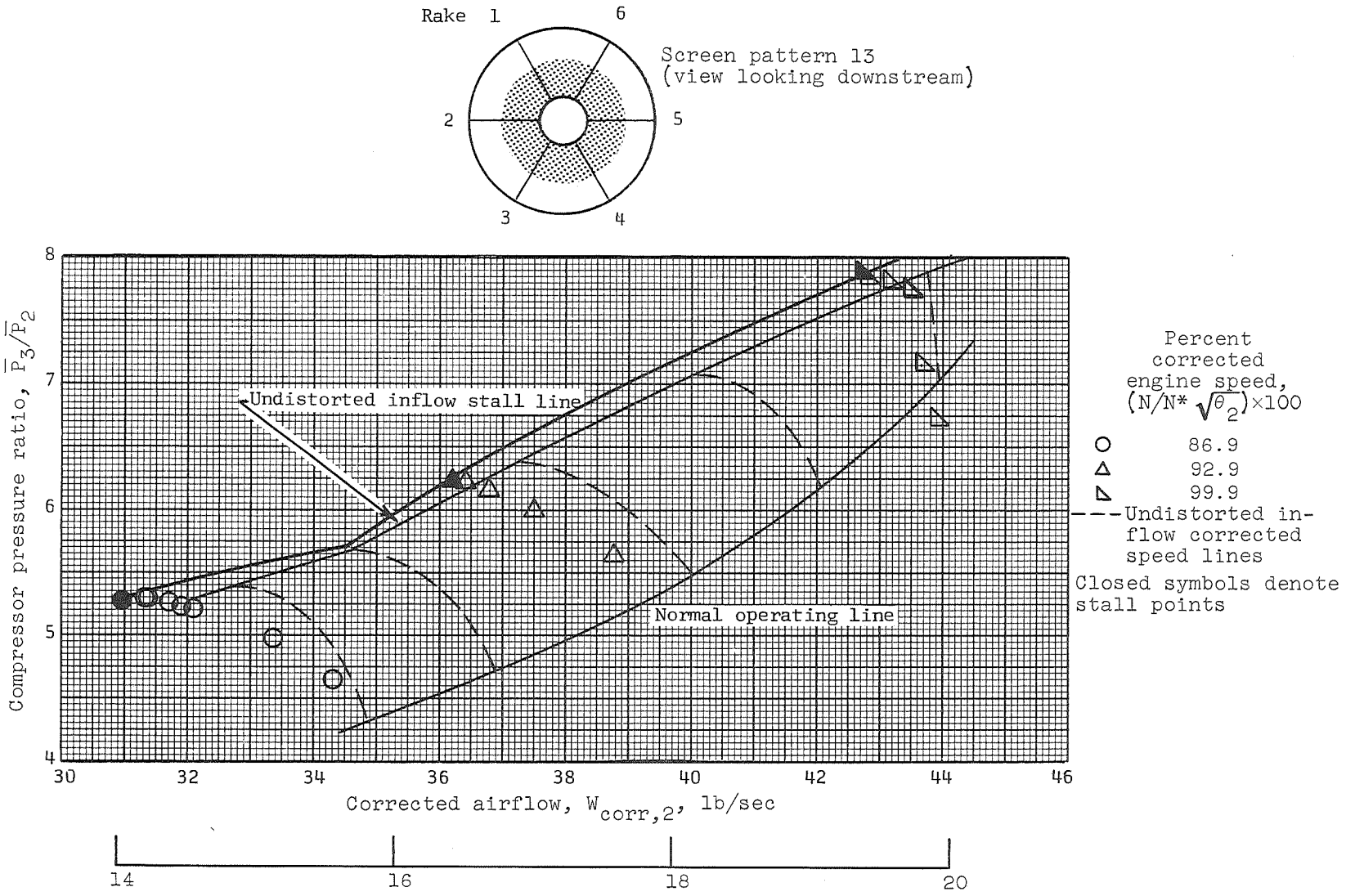


(b) $7\frac{1}{2}$ mesh screen; $A_{sp}/A_2 = 0.4$.

Figure 9. - Continued.

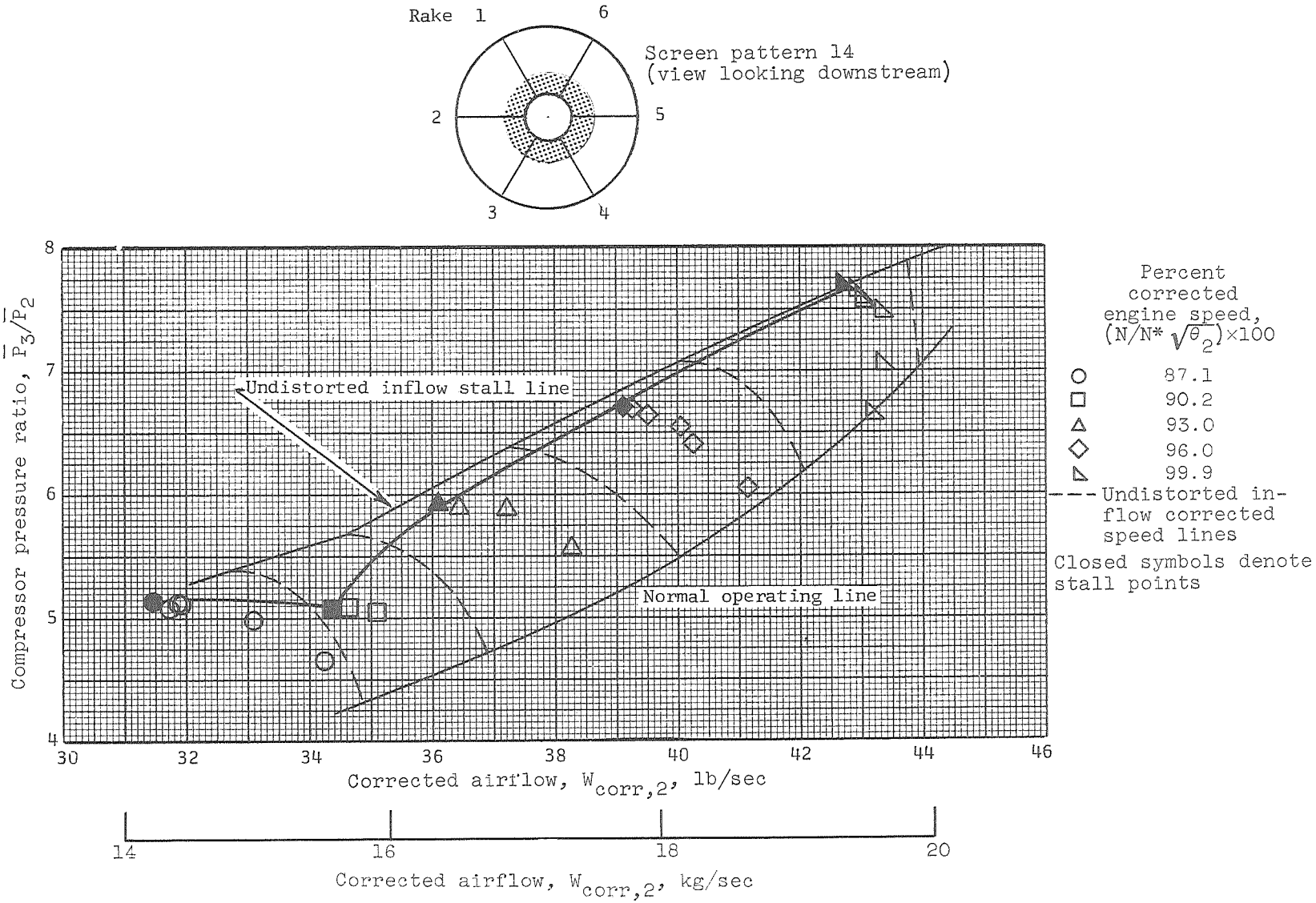


(c) 9 mesh screen; $A_{sp}/A_2 = 0.2$.

Figure 9. - Continued.

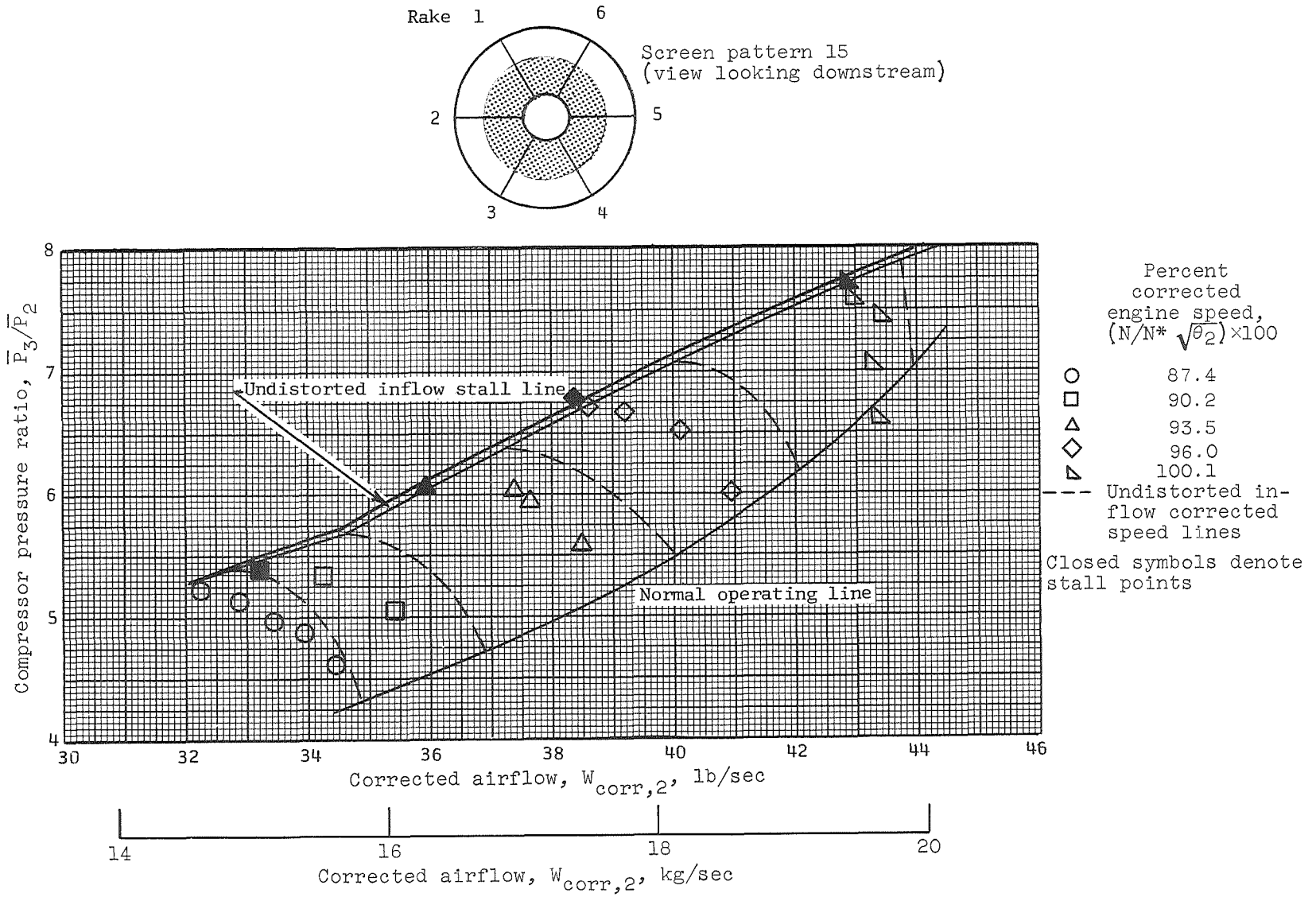


(d) 9 mesh screen; $A_{sp}/A_2 = 0.4$.

Figure 9. - Concluded.

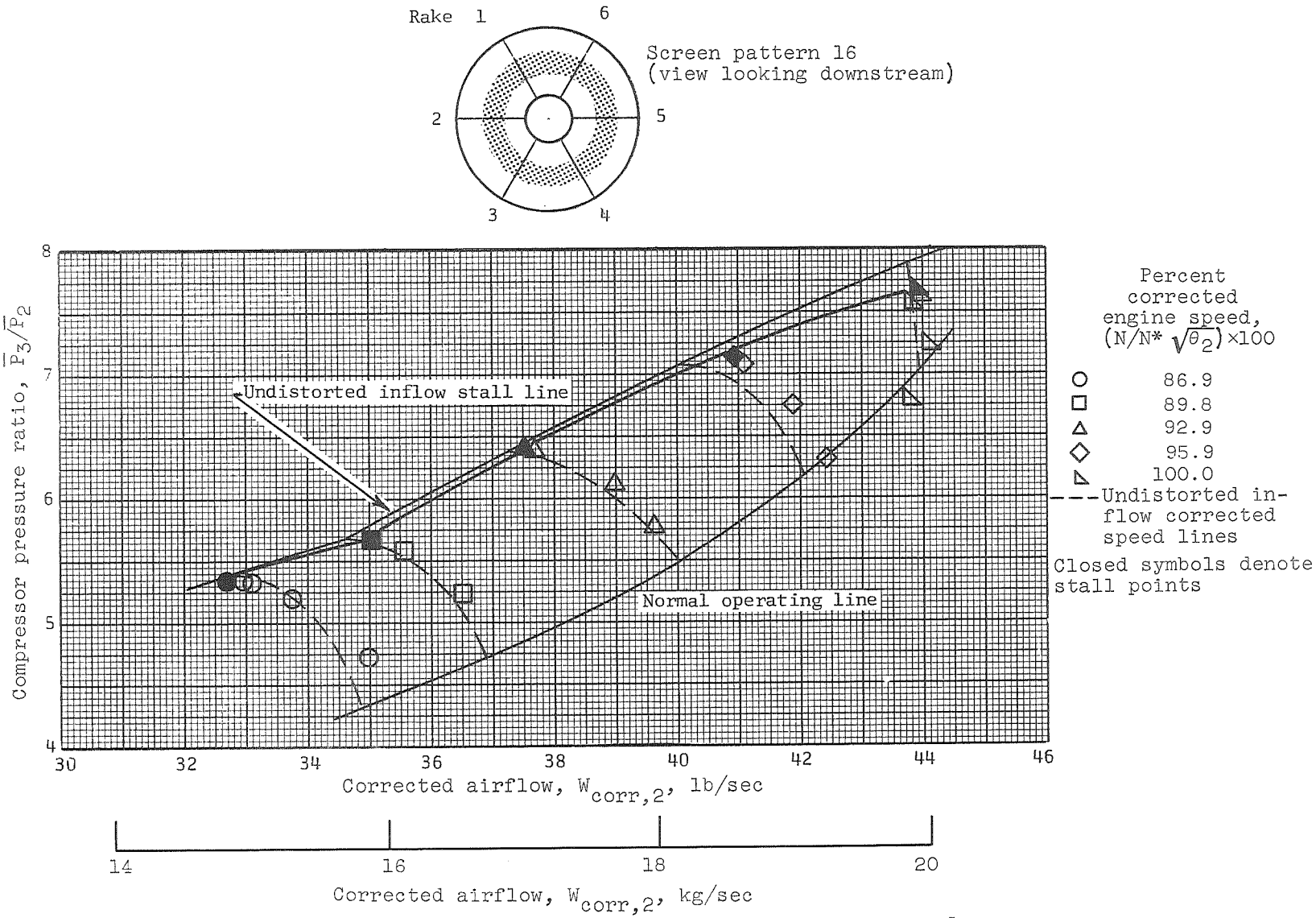


Figure 10. - Compressor performance with midspan radial distortion; $7\frac{1}{2}$ mesh screen; $A_{sp}/A_2 = 0.4$.

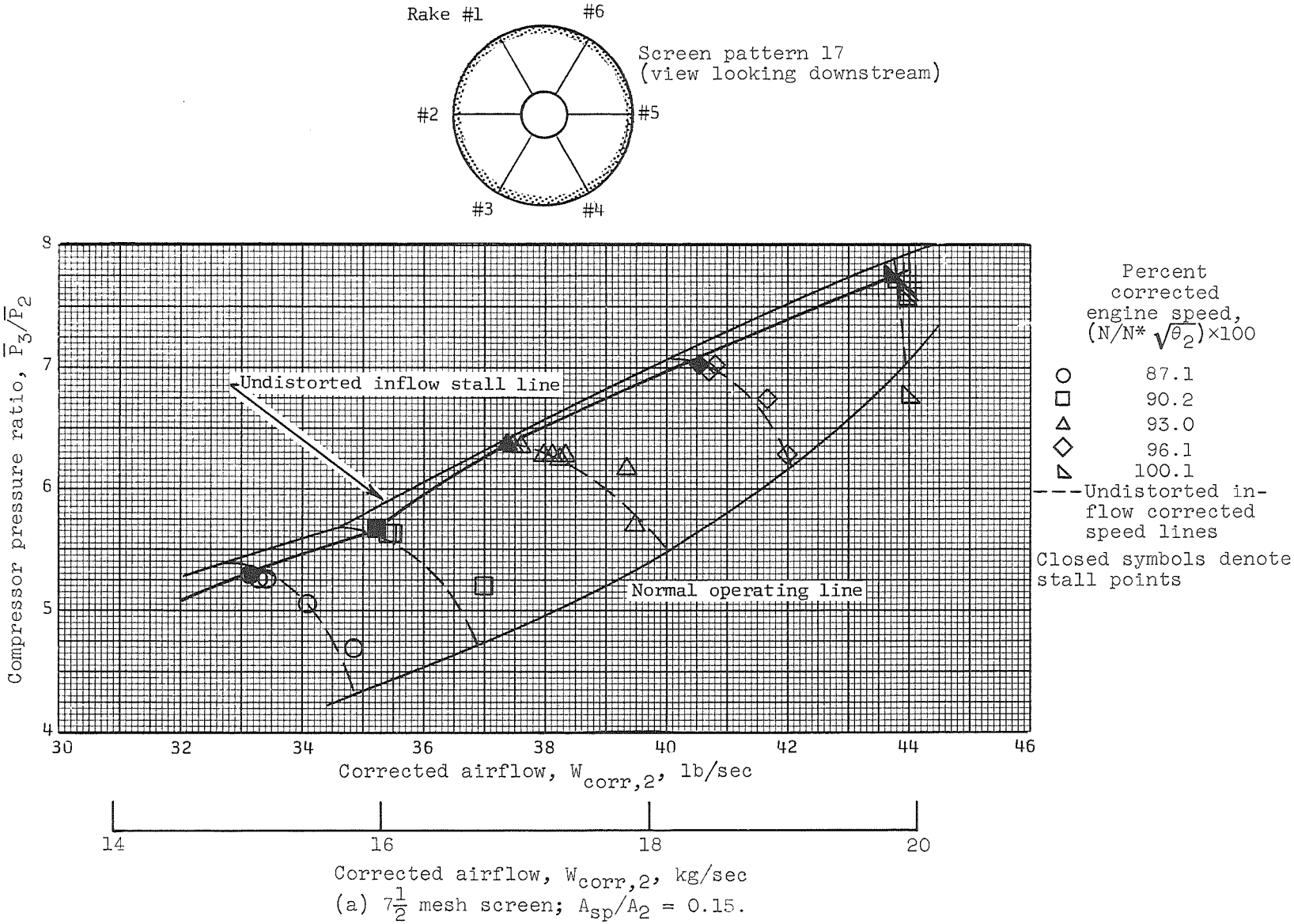


(a) $7\frac{1}{2}$ mesh screen; $A_{sp}/A_2 = 0.15$.

Figure 11. - Compressor performance with tip radial distortion.

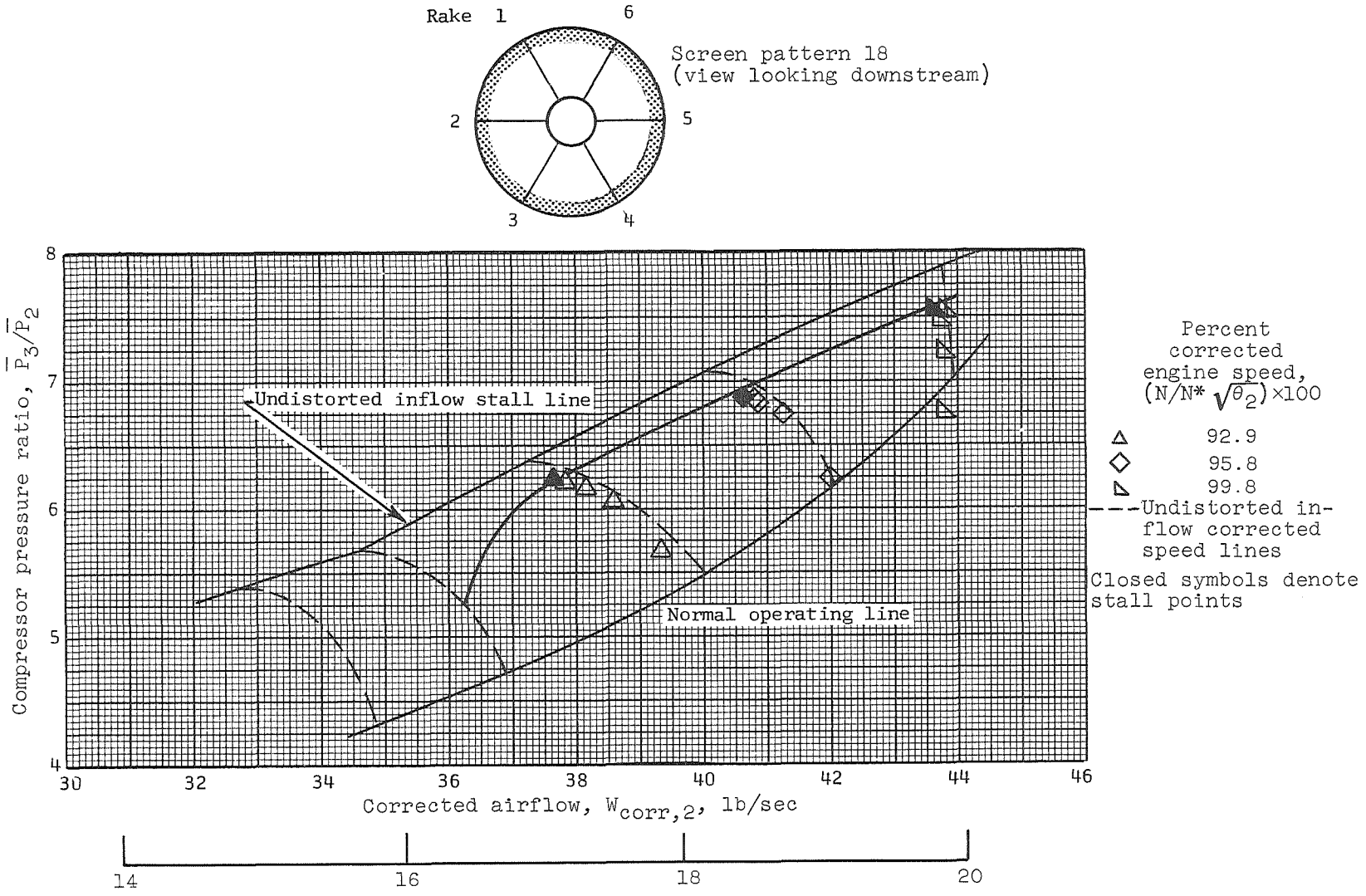


(b) $7\frac{1}{2}$ mesh screen; $A_{sp}/A_2 = 0.3$.

Figure 11. - Continued.

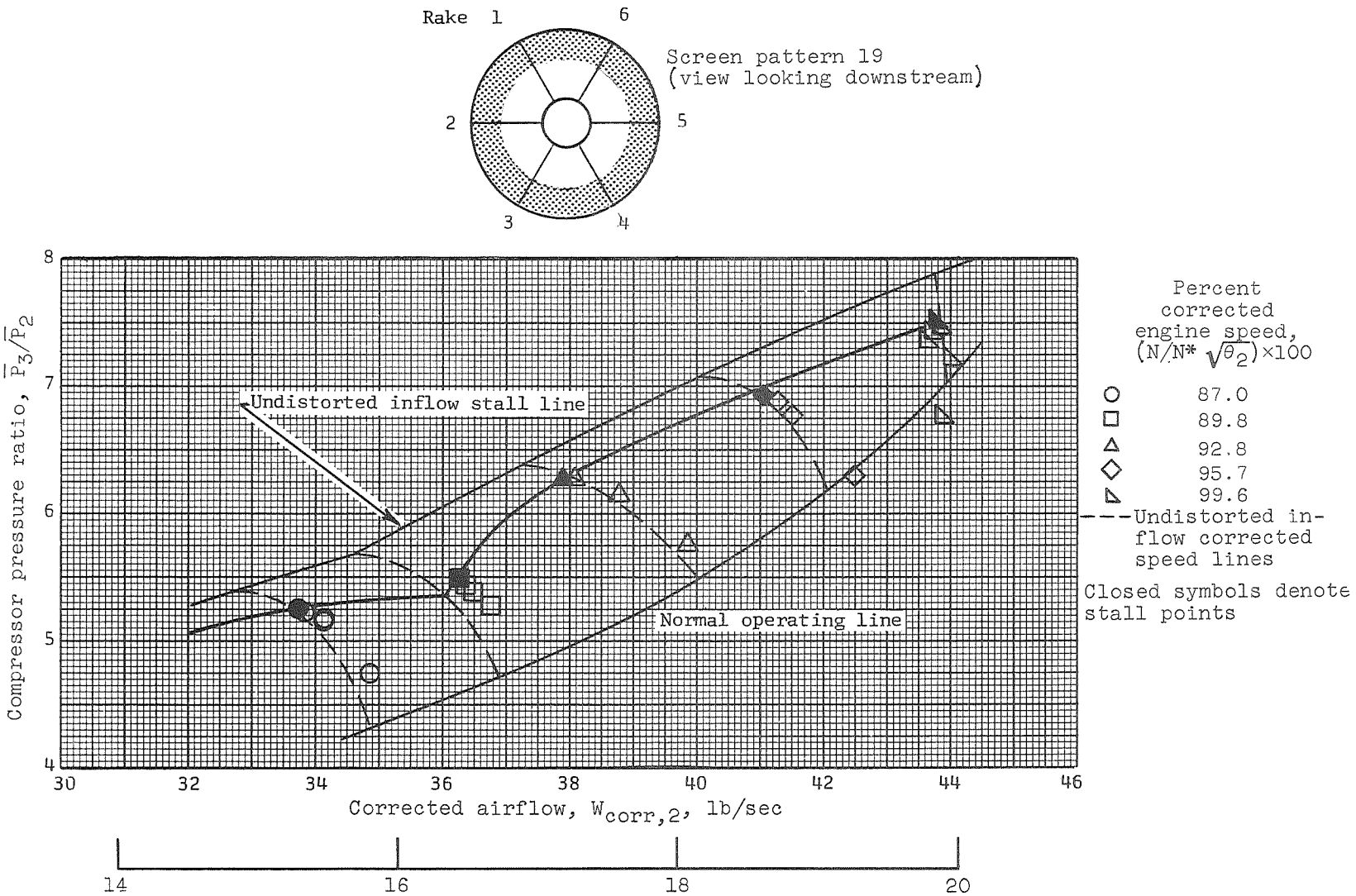


(c) $7\frac{1}{2}$ mesh screen; $A_{sp}/A_2 = 0.6$.

Figure 11. - Continued.

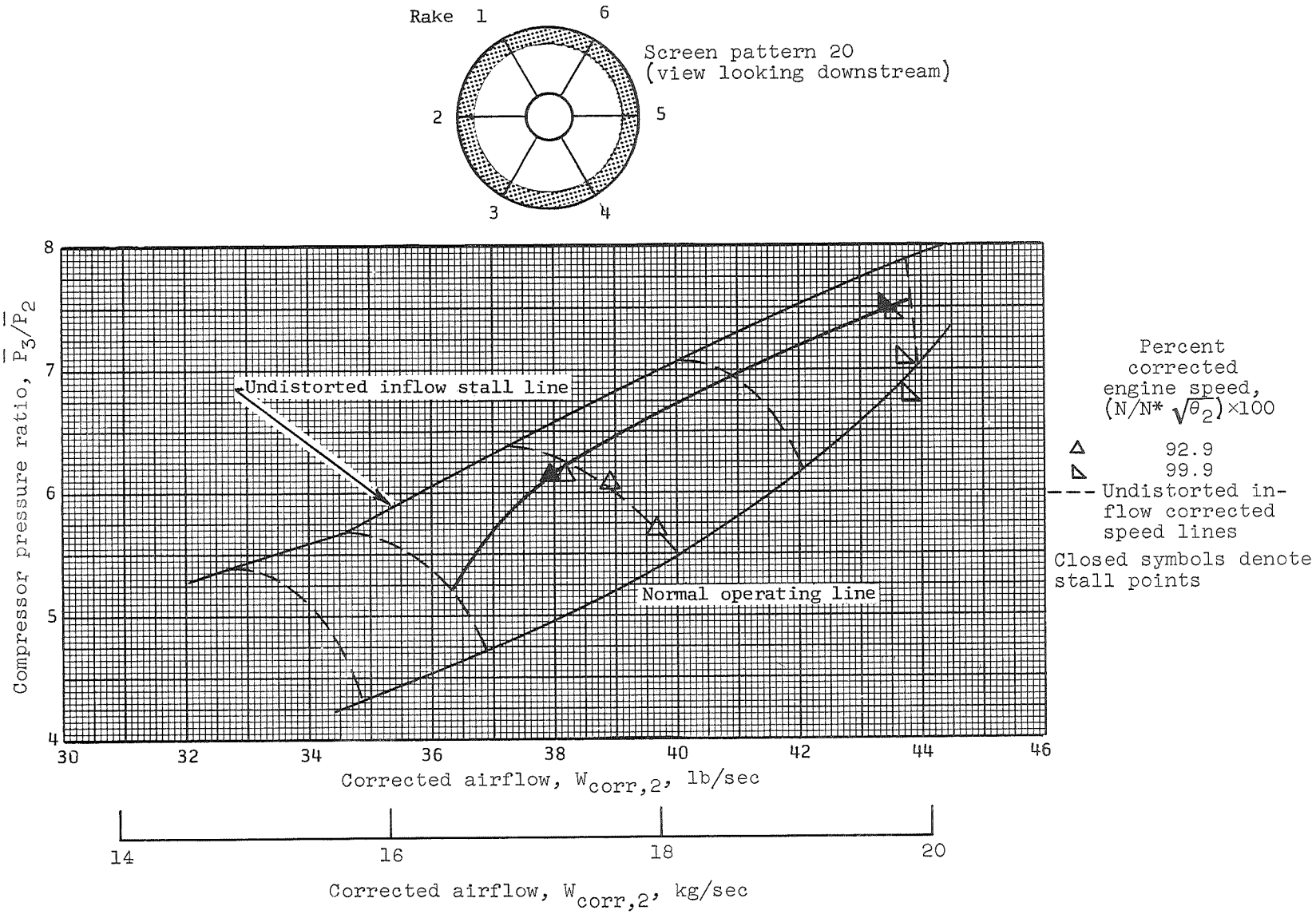


(d) $8\frac{1}{2}$ mesh screen; $A_{sp}/A_2 = 0.3$.

Figure 11. - Continued.

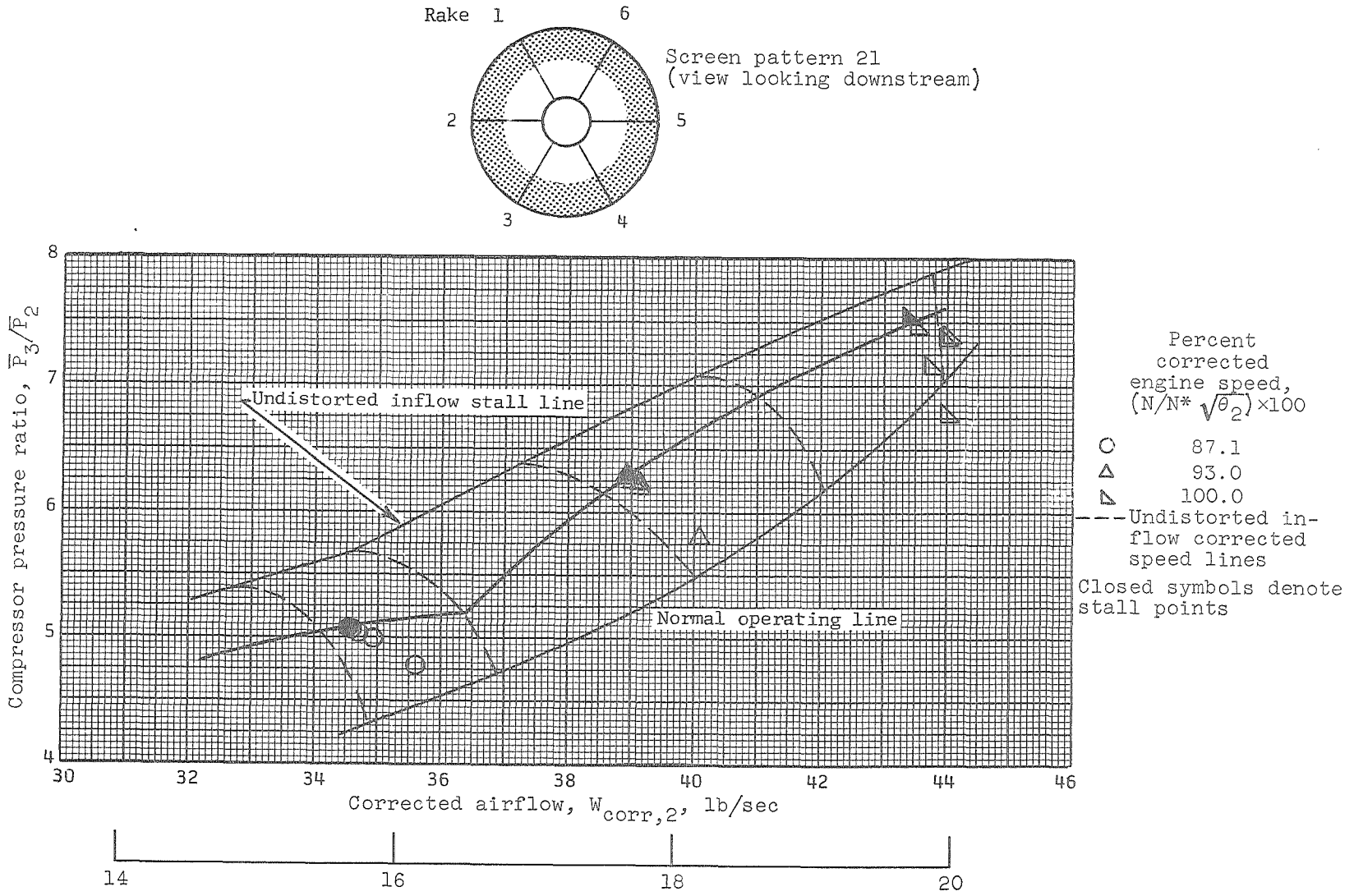


(e) $8\frac{1}{2}$ mesh screen; $A_{sp}/A_2 = 0.6$.

Figure 11. - Concluded.

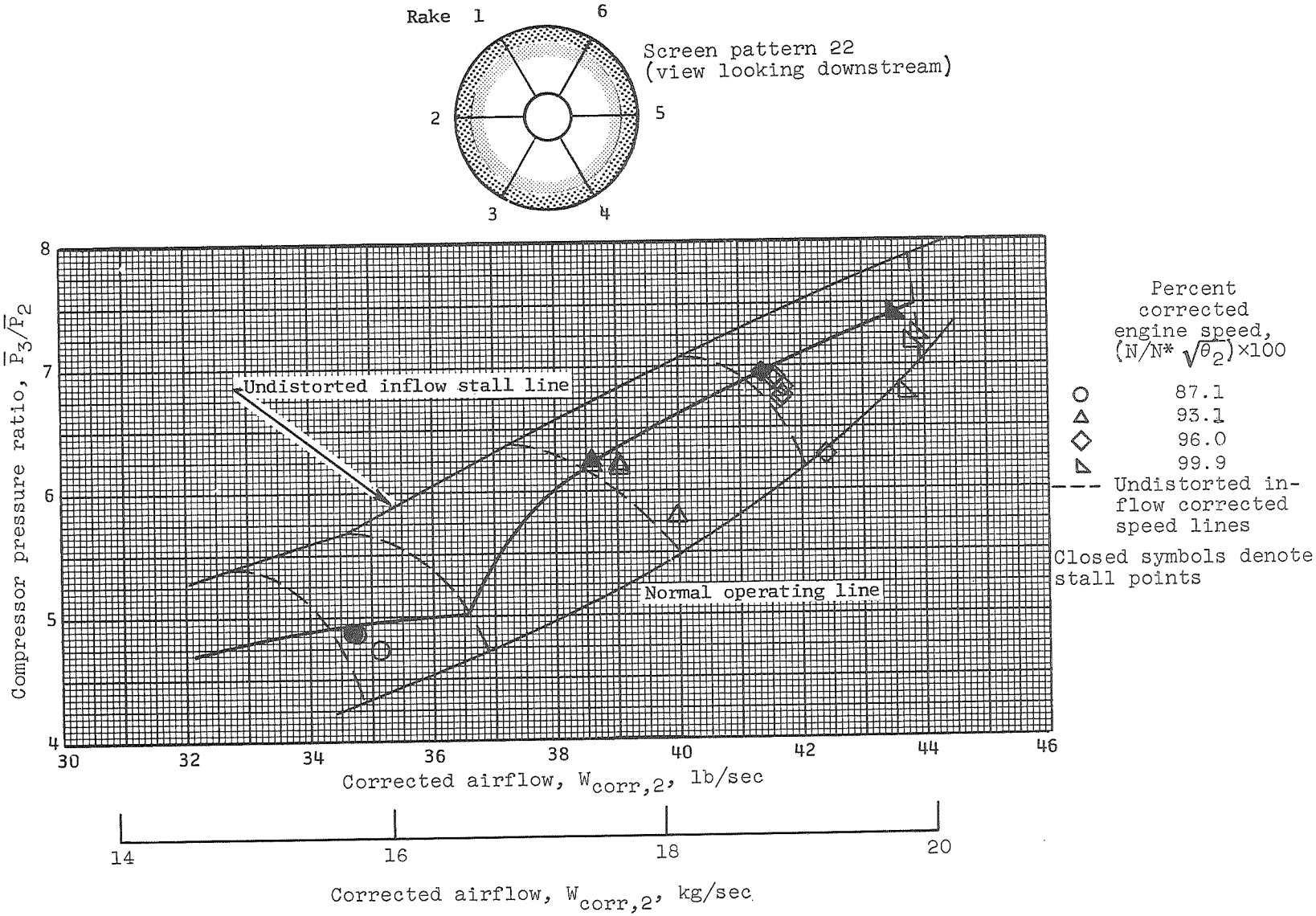


Figure 12. - Compressor performance with graded tip radial distortion screens. Outermost annulus: $8\frac{1}{2}$ mesh, $A_{sp}/A_2 = 0.3$; inner annulus: $7\frac{1}{2}$ mesh, $A_{sp}/A_2 = 0.3$.

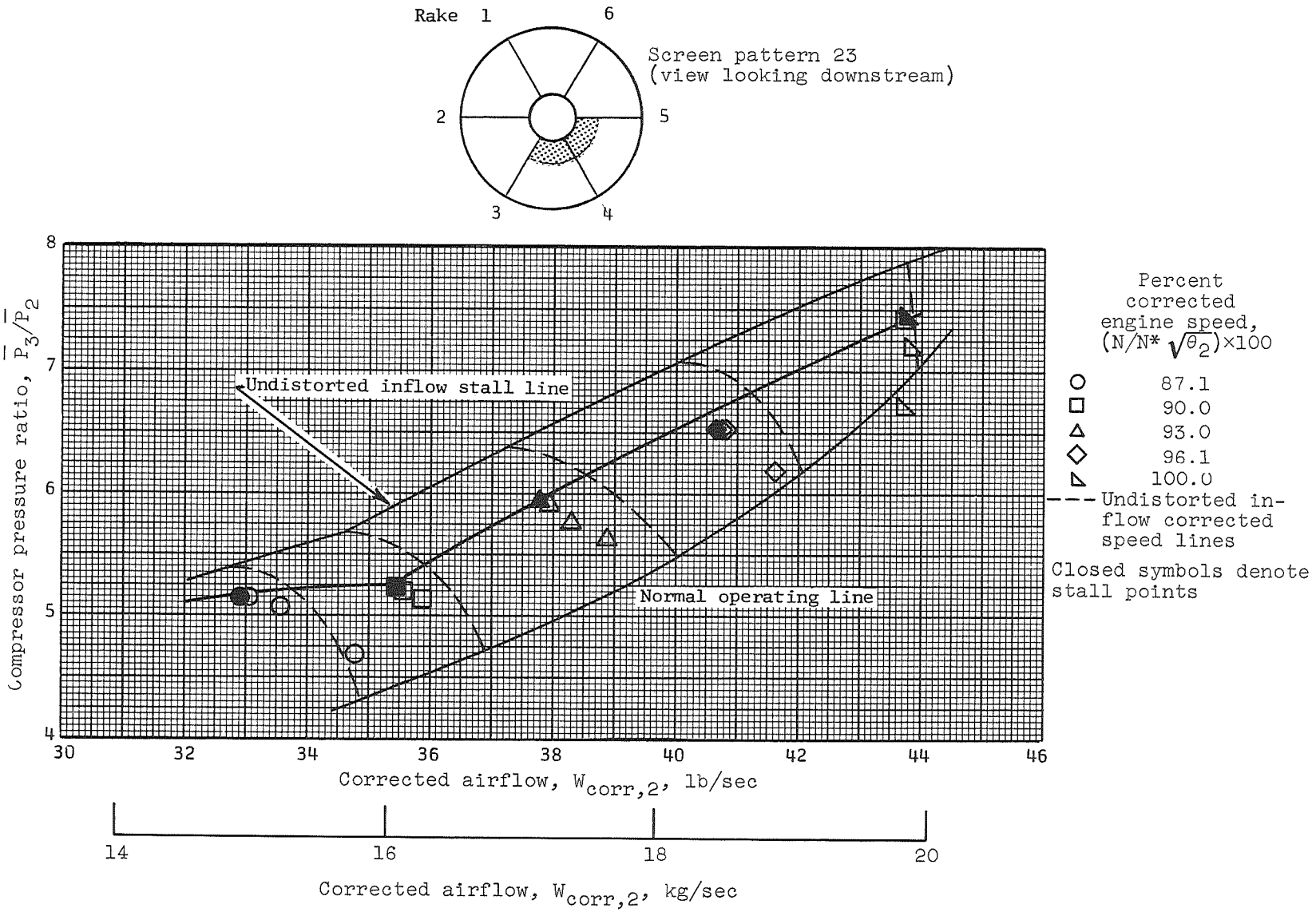


Figure 13. - Compressor performance with 120° sector of hub radial distortion; 9 mesh screen; $A_{sp}/A_2 = 0.067$.

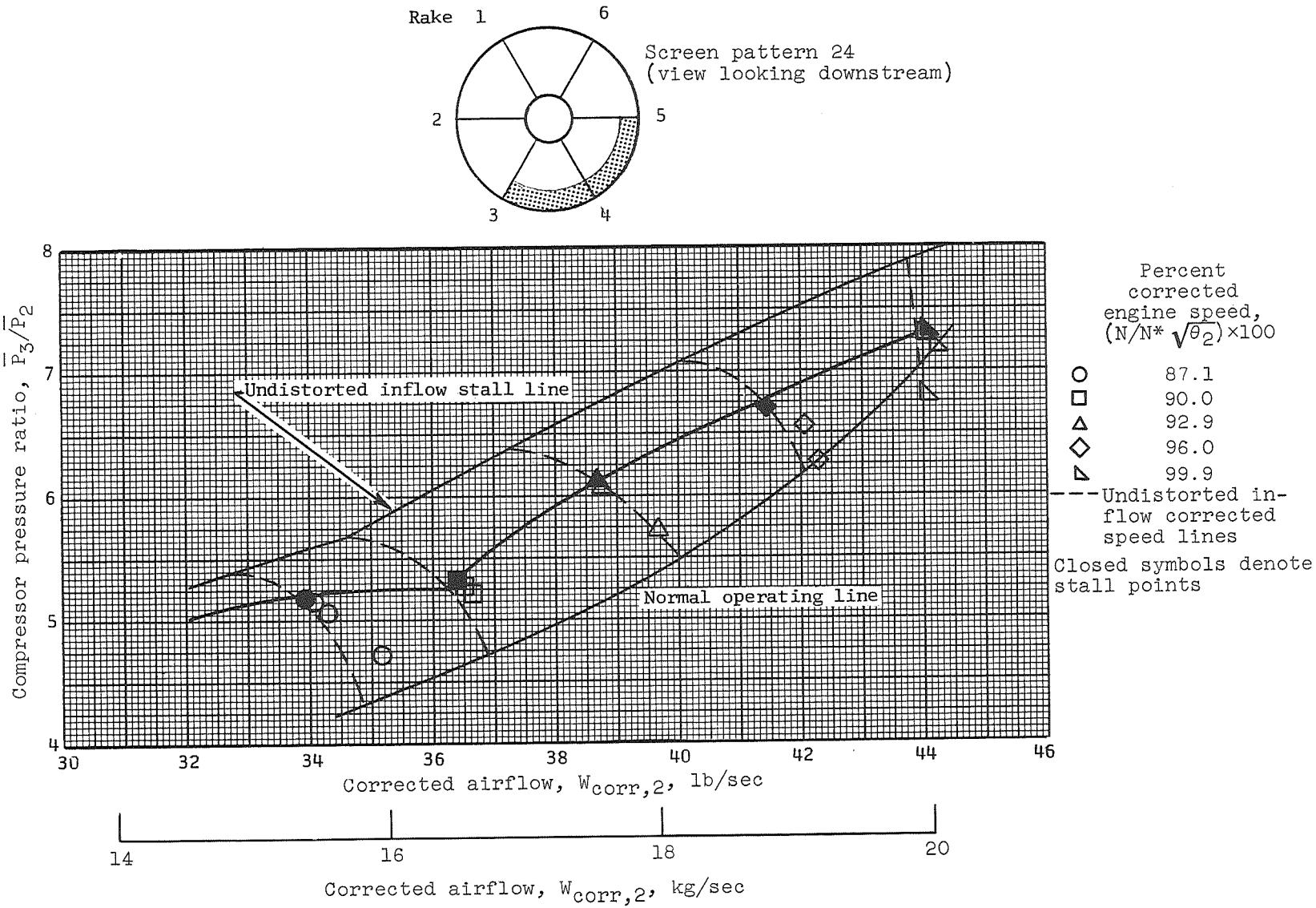


Figure 14. - Compressor performance with 120° sector of tip radial distortion; 9 mesh screen; $A_{sp}/A_2 = 0.133$.

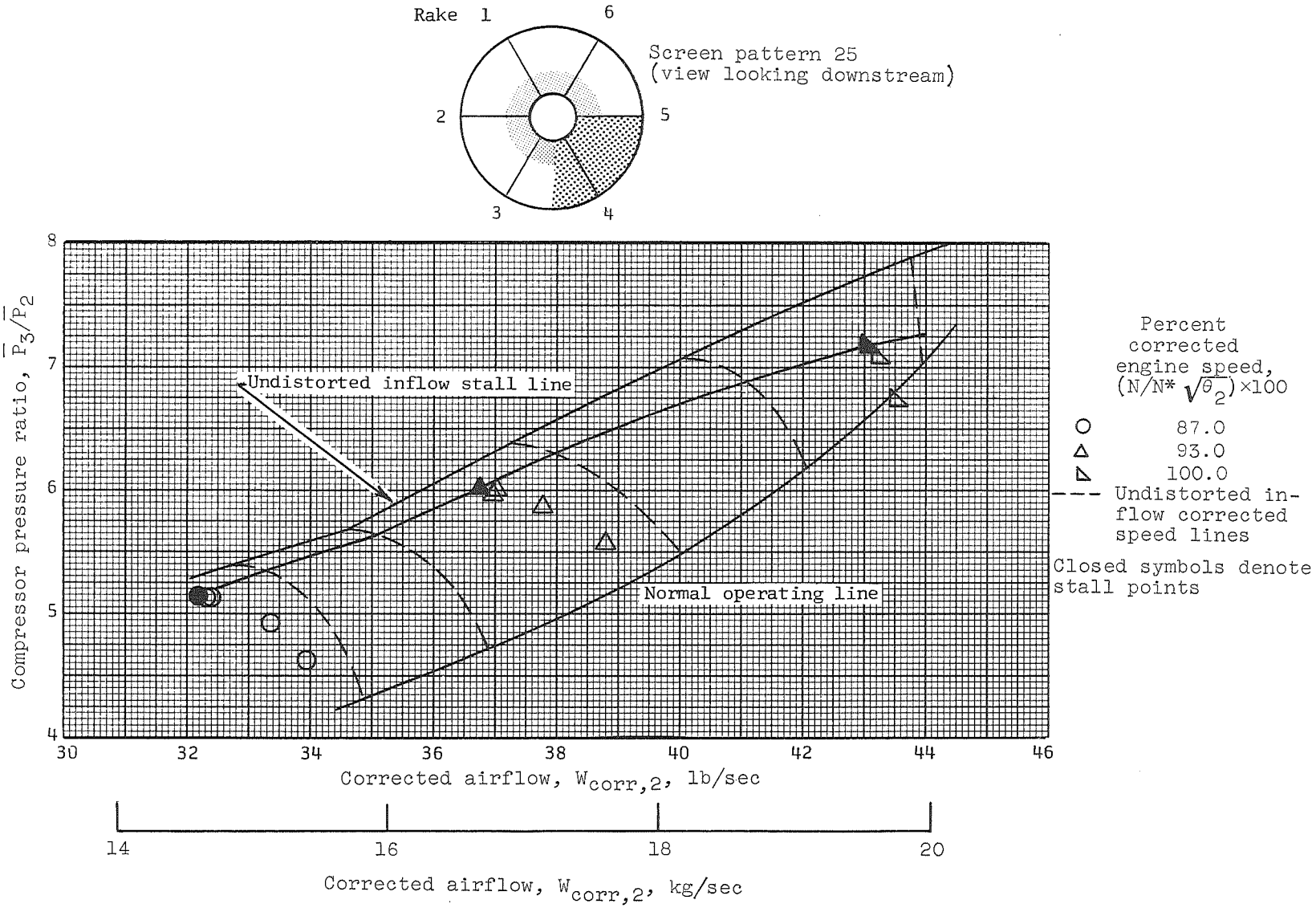


Figure 15. - Compressor performance with 270° hub radial and 90° circumferential distortion; radial sector: $7\frac{1}{2}$ mesh screen; $A_{sp}/A_2 = 0.15$; circumferential sector: $8\frac{1}{2}$ mesh screen.

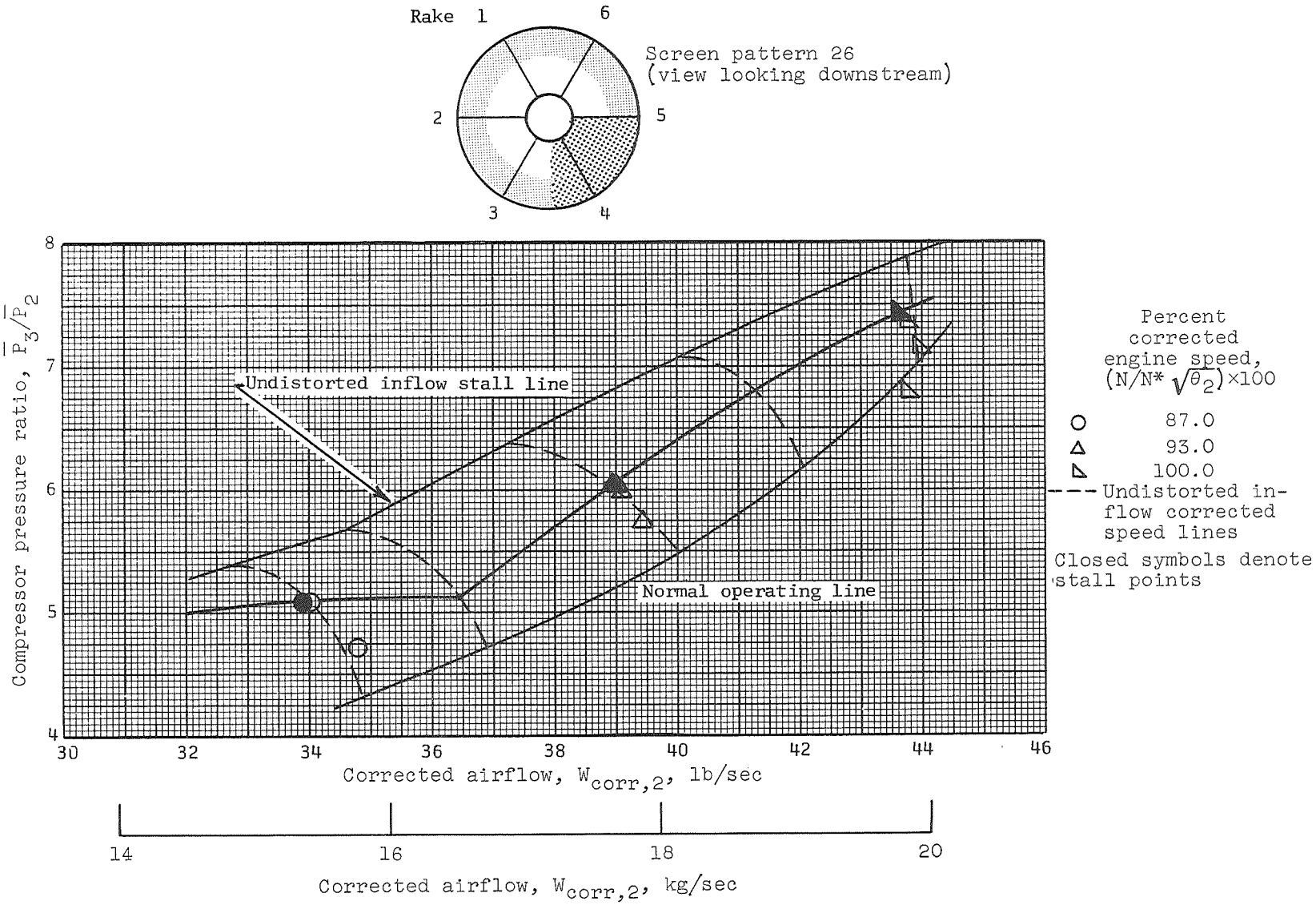


Figure 16. - Compressor performance with 270° tip radial and 90° circumferential distortion; radial sector: $7\frac{1}{2}$ mesh screen, $A_{sp}/A_2 = 0.45$; circumferential sector: $7\frac{1}{2}$ mesh screen.

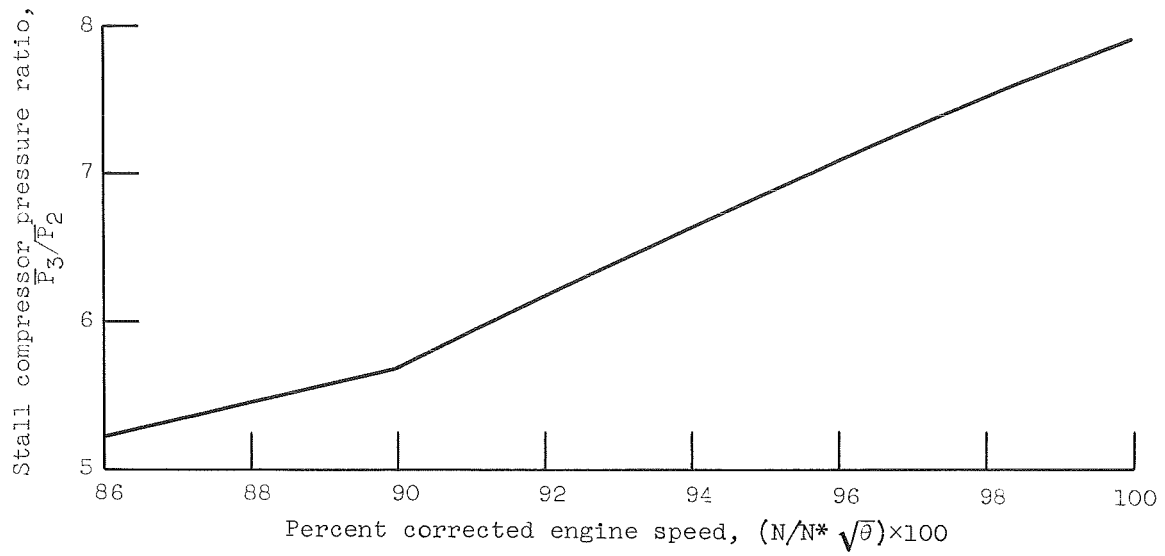


Figure 17. - Compressor pressure ratio at stall for undistorted inflow as a function of corrected engine speed.

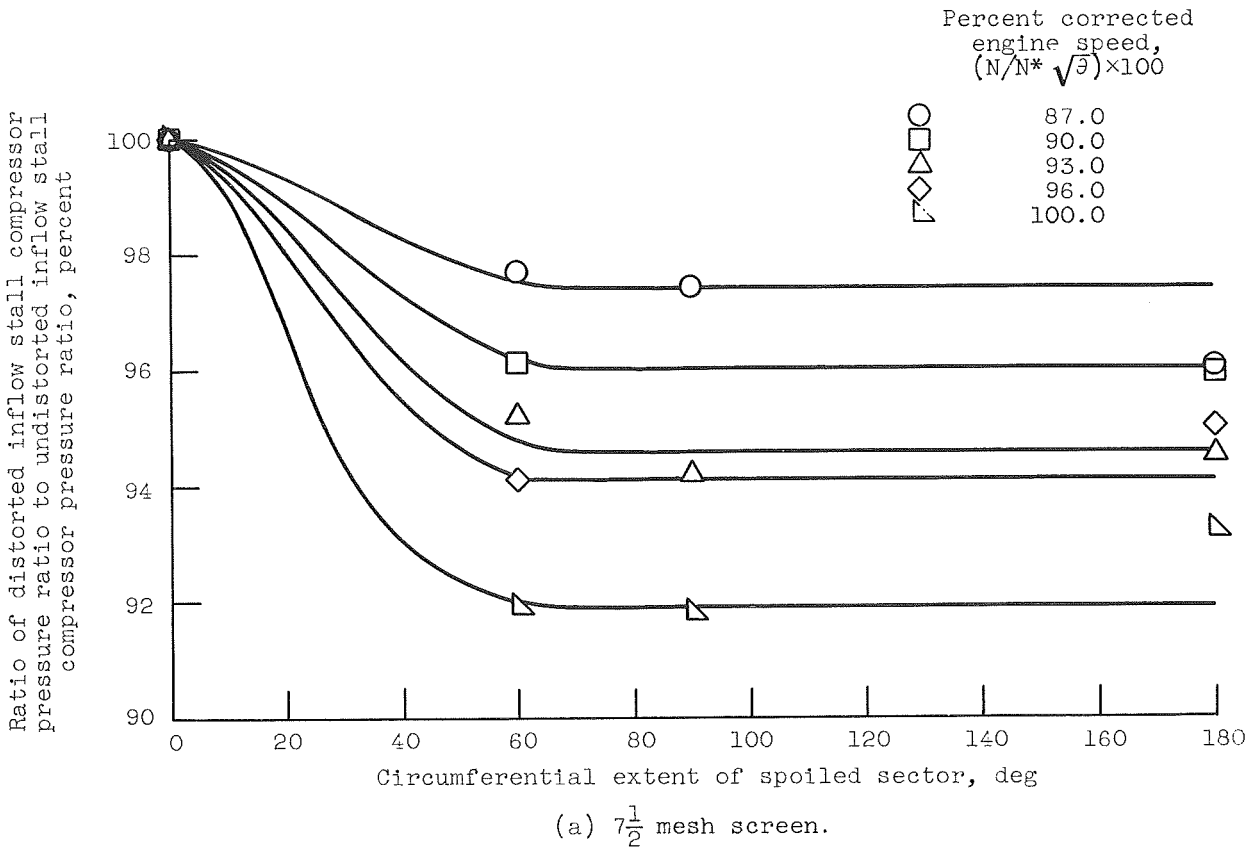


(a) $7\frac{1}{2}$ mesh screen.

Figure 18. - Effect of angle of circumferential spoiling on compressor stall.

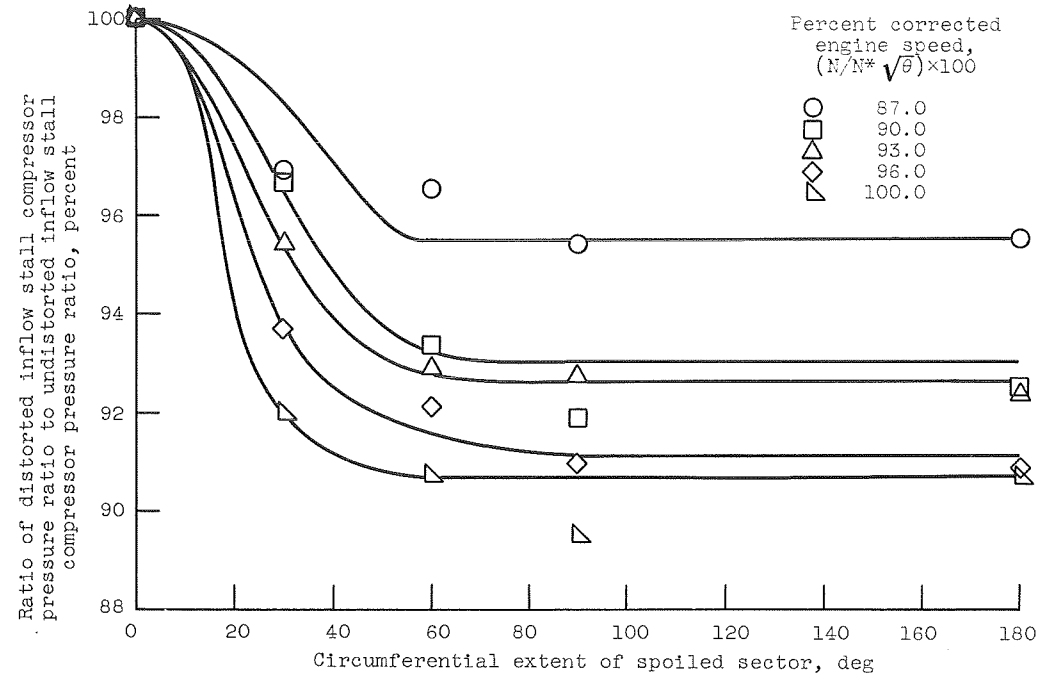


(b) $8\frac{1}{2}$ mesh screen.

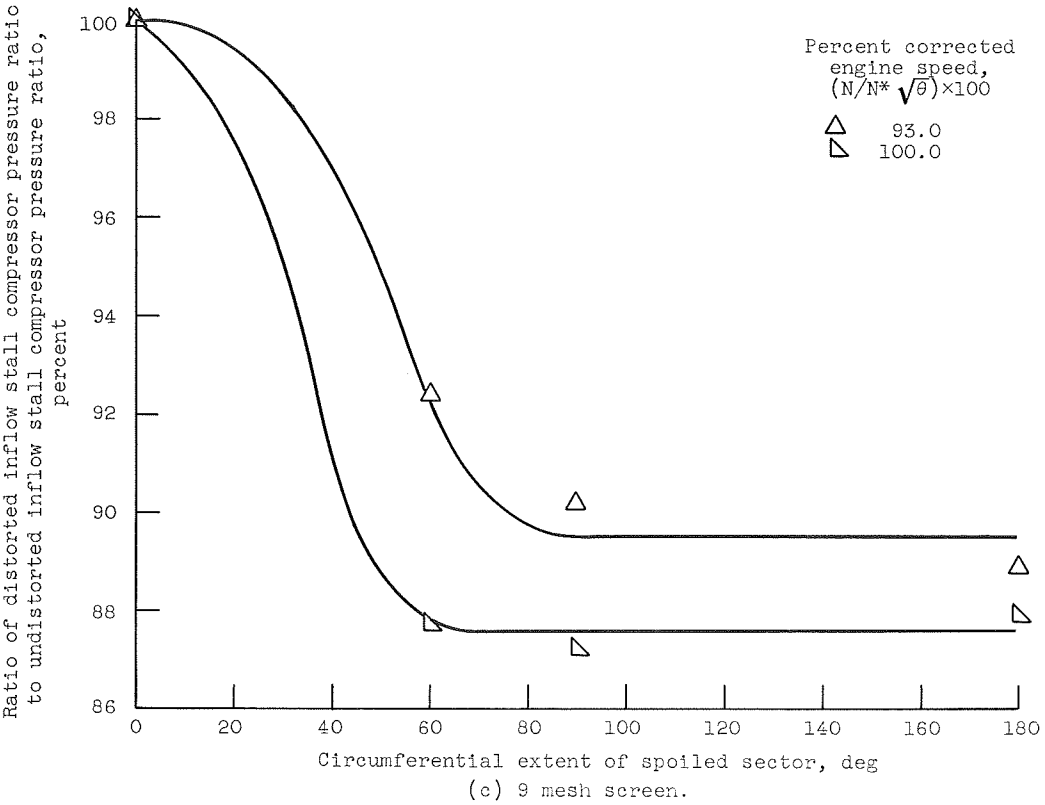


(c) 9 mesh screen.

Figure 18. - Concluded.

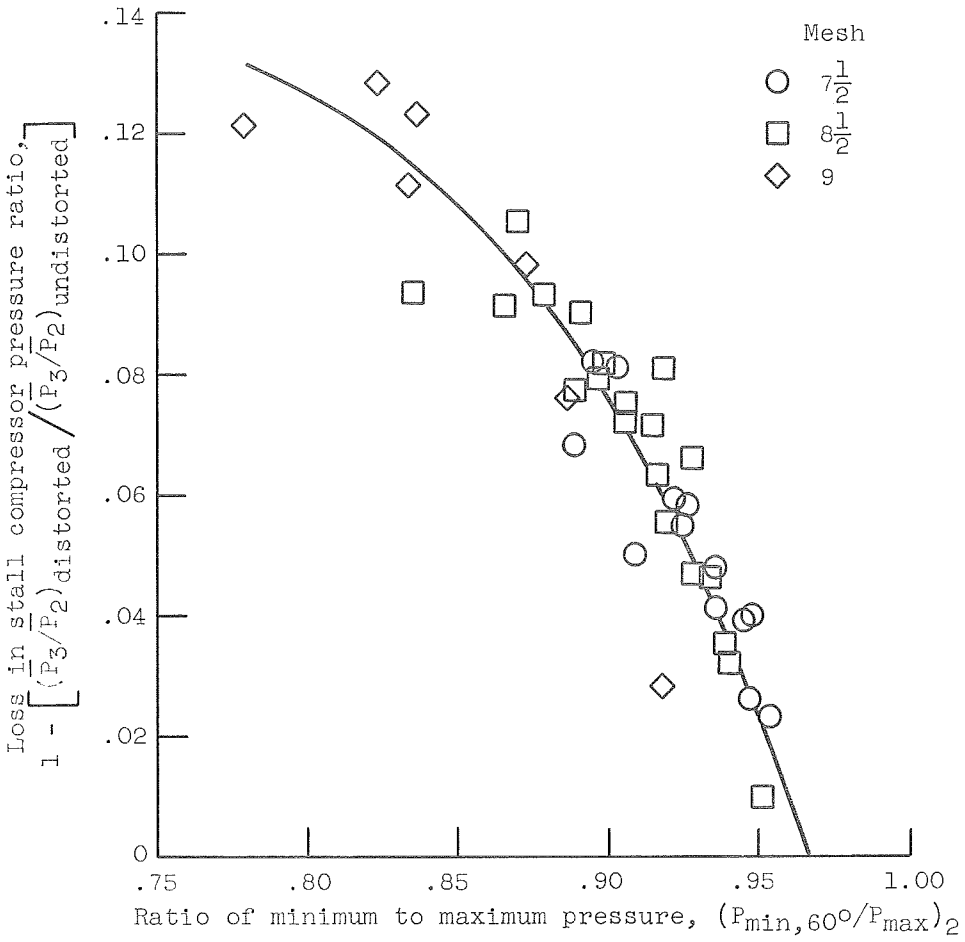


(a) Distortion index independent of circumferential extent.

Figure 19. - Effect of circumferential distortion on compressor stall.

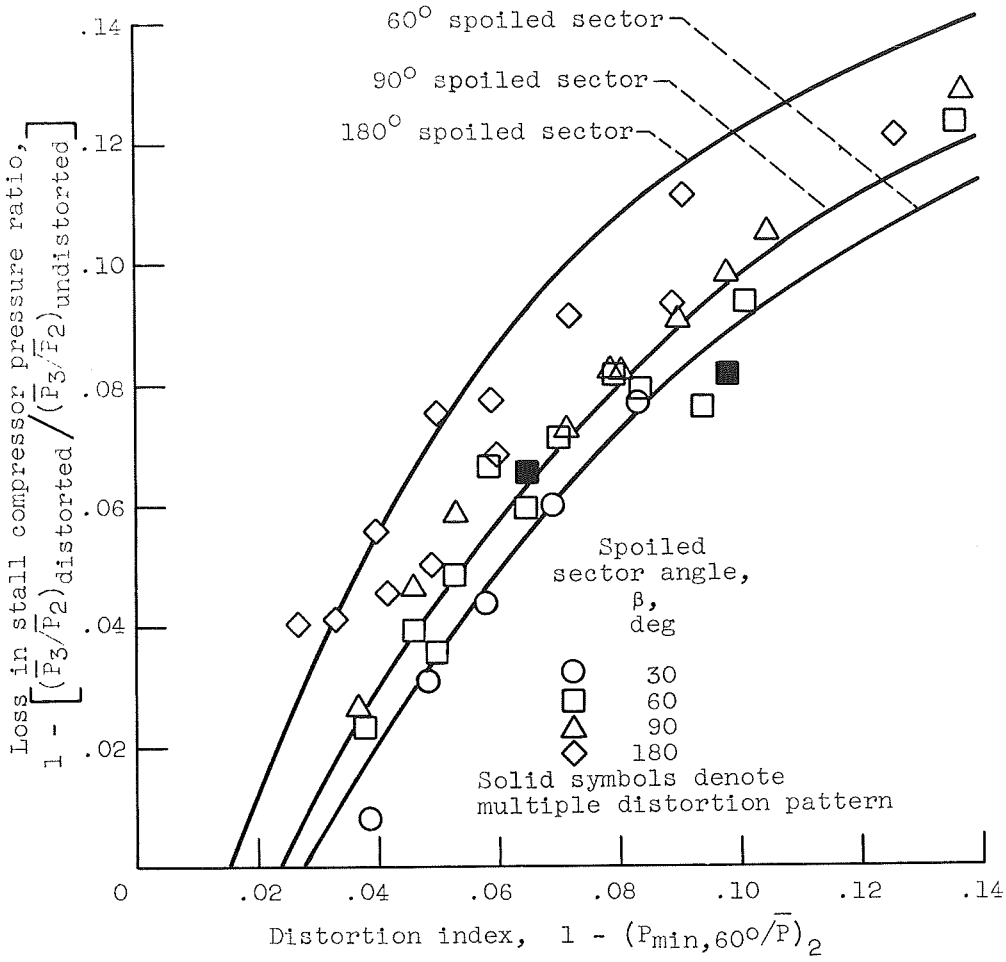


(b) Distortion index dependent on circumferential extent.

Figure 19. - Continued.

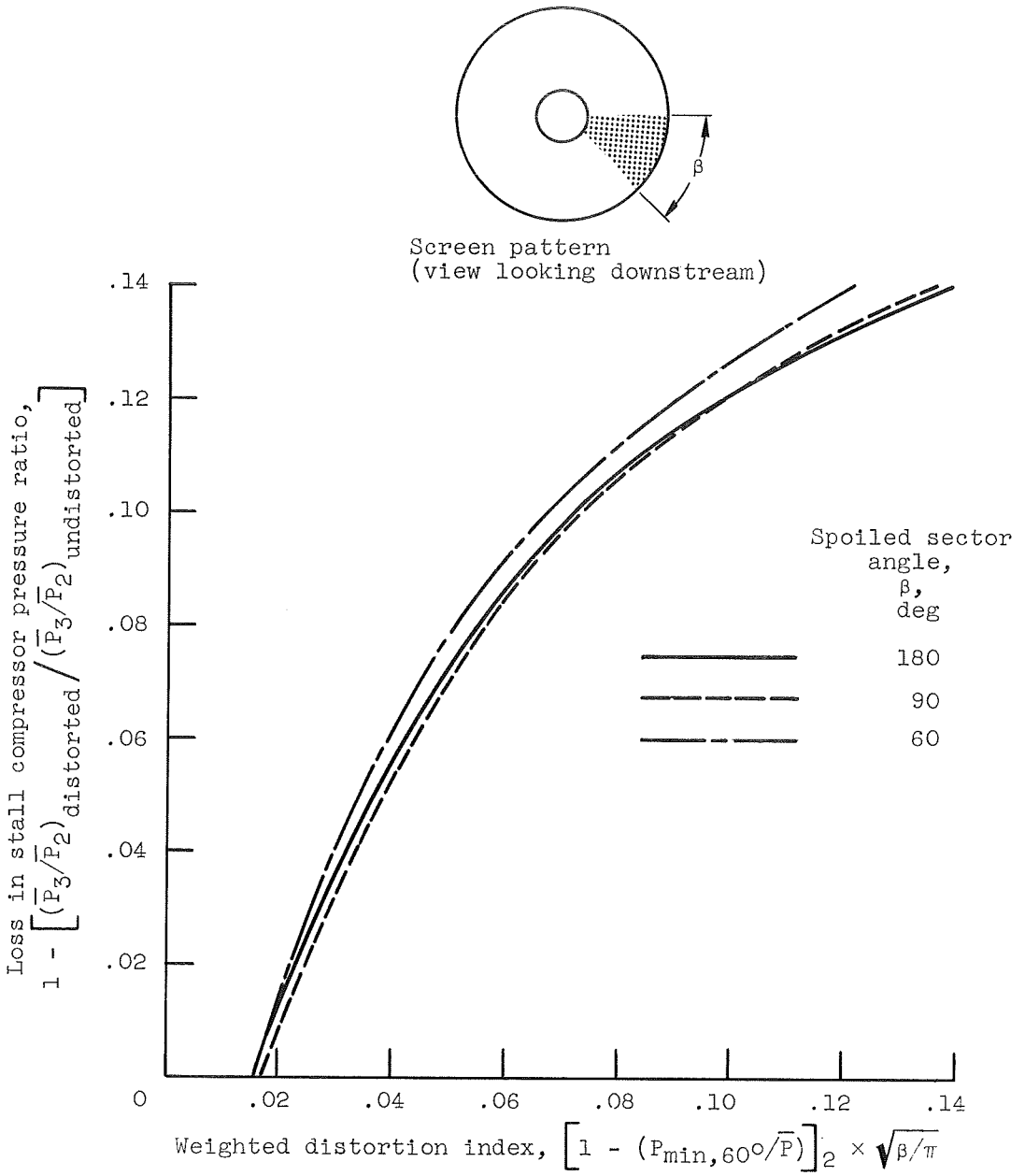


(c) Weighted distortion index.

Figure 19. - Concluded.

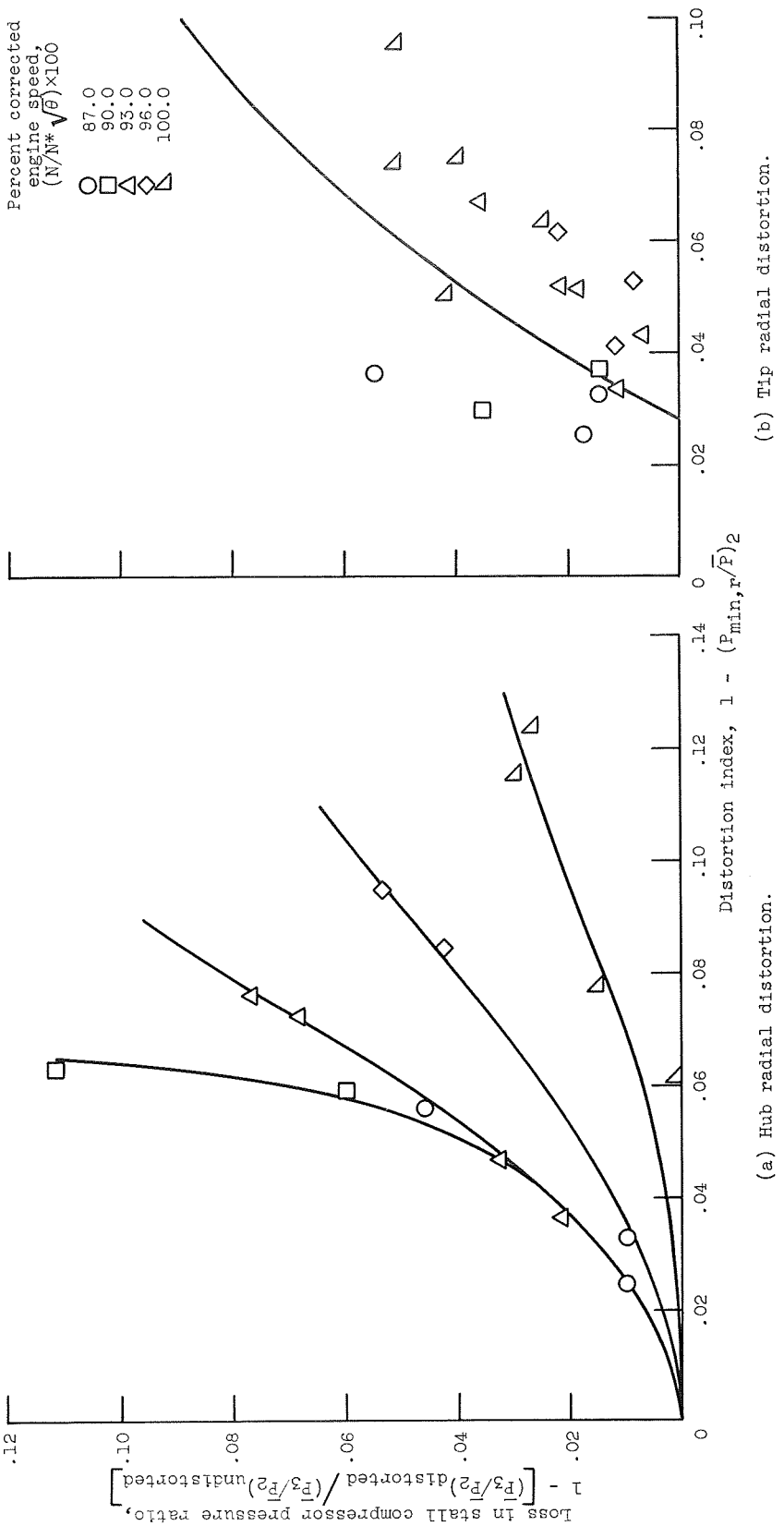


(a) Hub radial distortion.

(b) Tip radial distortion.

Figure 20. - Effect of radial distortion on compressor stall.

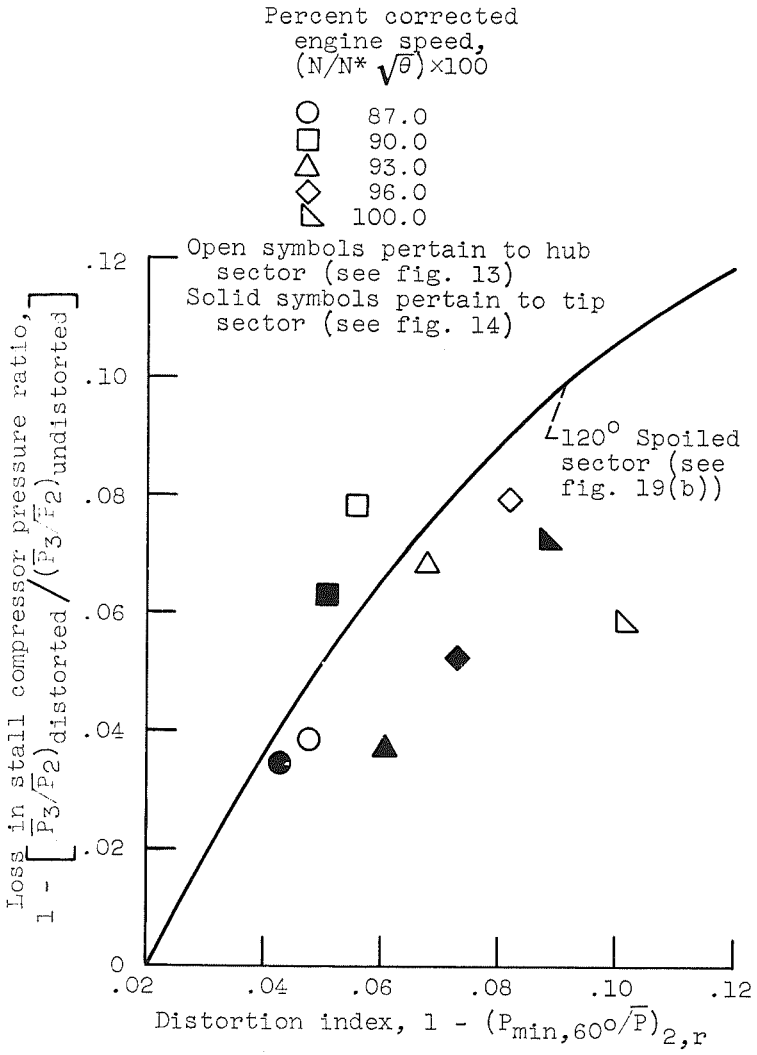


Figure 21. - Effect of 120° sectors of tip and hub radial distortions on compressor stall.

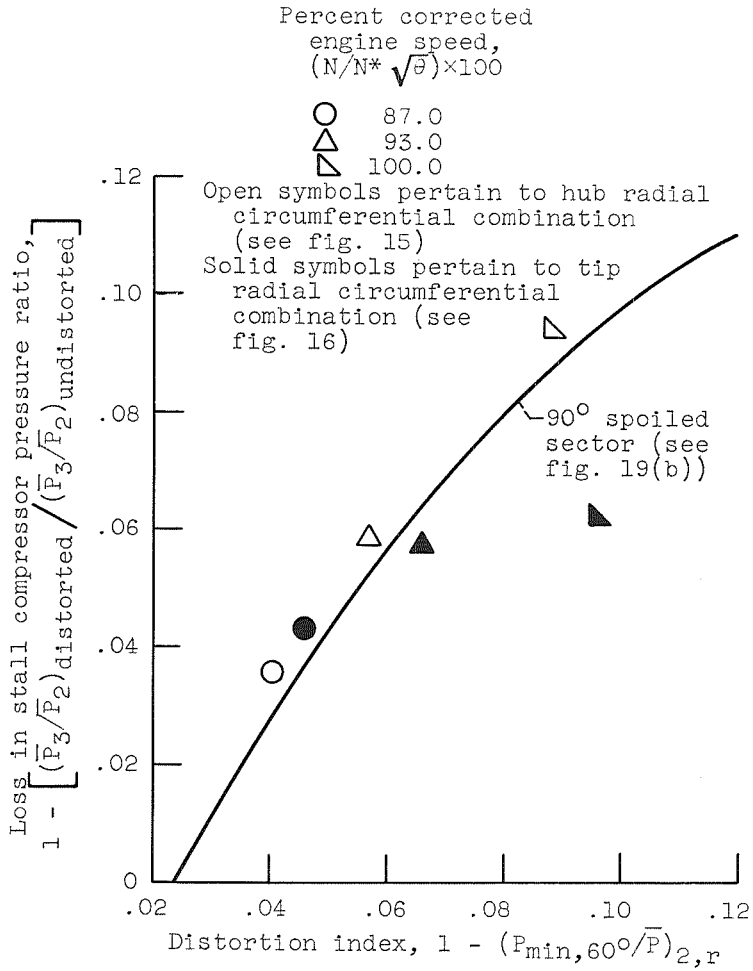


Figure 22. - Effect of 270° radial, 90° circumferential distortion combinations on compressor stall.

*"The aeronautical and space activities of the United States shall be conducted so as to contribute . . . to the expansion of human knowledge of phenomena in the atmosphere and space. The Administration shall provide for the widest practicable and appropriate dissemination of information concerning its activities and the results thereof."*

—NATIONAL AERONAUTICS AND SPACE ACT OF 1958

# NASA SCIENTIFIC AND TECHNICAL PUBLICATIONS

TECHNICAL REPORTS: Scientific and technical information considered important, complete, and a lasting contribution to existing knowledge.

TECHNICAL NOTES: Information less broad in scope but nevertheless of importance as a contribution to existing knowledge.

TECHNICAL MEMORANDUMS: Information receiving limited distribution because of preliminary data, security classification, or other reasons.

CONTRACTOR REPORTS: Scientific and technical information generated under a NASA contract or grant and considered an important contribution to existing knowledge.

TECHNICAL TRANSLATIONS: Information published in a foreign language considered to merit NASA distribution in English.

SPECIAL PUBLICATIONS: Information derived from or of value to NASA activities. Publications include conference proceedings, monographs, data compilations, handbooks, sourcebooks, and special bibliographies.

TECHNOLOGY UTILIZATION PUBLICATIONS: Information on technology used by NASA that may be of particular interest in commercial and other non-aerospace applications. Publications include Tech Briefs, Technology Utilization Reports and Technology Surveys.

*Details on the availability of these publications may be obtained from:*

SCIENTIFIC AND TECHNICAL INFORMATION OFFICE

NATIONAL AERONAUTICS AND SPACE ADMINISTRATION

**Washington, D.C. 20546**